Dynamical Seasonal Prediction of Tropical Cyclone Activity Using the FGOALS-f2 Ensemble Prediction System

JINXIAO LI,[a] QING BAO,[a] YIMIN LIU,[a] GUOXIONG WU,[a] LEI WANG,[a] BIAN HE,[a] XIAOCONG WANG,[a] JING YANG,[b] XIAOFEI WU,[c] AND ZILI SHEN[d]

[a] *State Key Laboratory of Numerical Modeling for Atmospheric Sciences and Geophysical Fluid Dynamics, Institute of Atmospheric Physics, Chinese Academy of Sciences, Beijing, China*
[b] *State Key Laboratory of Earth Surface Processes and Resource Ecology, Faculty of Geographical Science, Beijing Normal University, Beijing, China*
[c] *School of Atmospheric Sciences/Plateau Atmosphere and Environment Key Laboratory of Sichuan Province, Chengdu University of Information Technology, Chengdu, China*
[d] *Collaborative Innovation Center on Forecast and Evaluation of Meteorological Disasters, Nanjing University of Information Science and Technology, Nanjing, China*

(Manuscript received 20 October 2020, in final form 6 June 2021)

ABSTRACT: There is a distinct gap between tropical cyclone (TC) prediction skill and the societal demand for accurate predictions, especially in the western Pacific (WP) and North Atlantic (NA) basins, where densely populated areas are frequently affected by intense TC events. In this study, seasonal prediction skill for TC activity in the WP and NA of the fully coupled FGOALS-f2 V1.0 dynamical prediction system is evaluated. In total, 36 years of monthly hindcasts from 1981 to 2016 were completed with 24 ensemble members. The FGOALS-f2 V1.0 system has been used for real-time predictions since June 2017 with 35 ensemble members, and has been operationally used in the two operational prediction centers of China. Our evaluation indicates that FGOALS-f2 V1.0 can reasonably reproduce the density of TC genesis locations and tracks in the WP and NA. The model shows significant skill in terms of the TC number correlation in the WP (0.60) and the NA (0.61) from 1981 to 2015; however, the model underestimates accumulated cyclone energy. When the number of ensemble members was increased from 2 to 24, the correlation coefficients clearly increased (from 0.21 to 0.60 in the WP, and from 0.18 to 0.61 in the NA). FGOALS-f2 V1.0 also successfully reproduces the genesis potential index pattern and the relationship between El Niño–Southern Oscillation and TC activity, which is one of the dominant contributors to TC seasonal prediction skill. However, the biases in large-scale factors are barriers to the improvement of the seasonal prediction skill, e.g., larger wind shear, higher relative humidity, and weaker potential intensity of TCs. For real-time predictions in the WP, FGOALS-f2 V1.0 demonstrates a skillful prediction for track density in terms of landfalling TCs, and the model successfully forecasts the correct sign of seasonal anomalies of landfalling TCs for various regions in China.

SIGNIFICANCE STATEMENT: Skillful prediction of tropical cyclone (TC) activity on a seasonal time scale is a reference for preventing and reducing disasters, but there is a distinct gap between TC prediction skill and the societal demand for accurate predictions, especially in the western Pacific and North Atlantic basins. The seasonal prediction of TCs using a global dynamical prediction system is potentially a useful tool for disaster prevention and mitigation. FGOALS-f2 V1.0 is a dynamical global ensemble prediction system, which has the ability to make seasonal predictions of global TCs. Here we evaluate the prediction skill for TCs in FGOALS-f2 V1.0 and then give possible reason(s) for the demonstrated levels of skill. The skillful prediction of TCs predicted by FGOALS-f2 V1.0 is shown in this study, especially in the western Pacific (WP) and the North Atlantic (NA), e.g., genesis location and TC number correlation (r = 0.60 in WP; r = 0.61 in NA), which will contribute to disaster prevention and mitigation.

KEYWORDS: Tropical cyclones; Seasonal forecasting; Climate models; Coupled models; Model evaluation/performance

1. Introduction

Seasonal prediction of tropical cyclone (TC) activity is of scientific value and is also a reference for disaster prevention and mitigation. Although the nowcasting of TC genesis locations and tracks is relatively accurate, it is difficult to satisfy the demands from all sectors of society, and a longer setup time is required for the prevention of high-impact TC events (Walsh et al. 2016; Camargo et al. 2007a; Camargo and Wing 2016; Vecchi et al. 2014). Seasonal forecasting is mainly concerned with the anomalies of a particular type of event compared to its climatology. The core mission of seasonal forecasting is to estimate the change in the likelihood of a climatic event happening in the next few months compared to its average

Denotes content that is immediately available upon publication as open access.

L. Wang's current affiliation: University of Chinese Academy of Sciences, Beijing, China.

Yang's current affiliation: Southern Marine Science and Engineering Guangdong Laboratory, Guangzhou, China.

Shen's current affiliation: State Key Laboratory of Numerical Modeling for Atmospheric Sciences and Geophysical Fluid Dynamics, Institute of Atmospheric Physics, Chinese Academy of Sciences, Beijing, China.

Corresponding author: Qing Bao, baoqing@mail.iap.ac.cn

DOI: 10.1175/WAF-D-20-0189.1

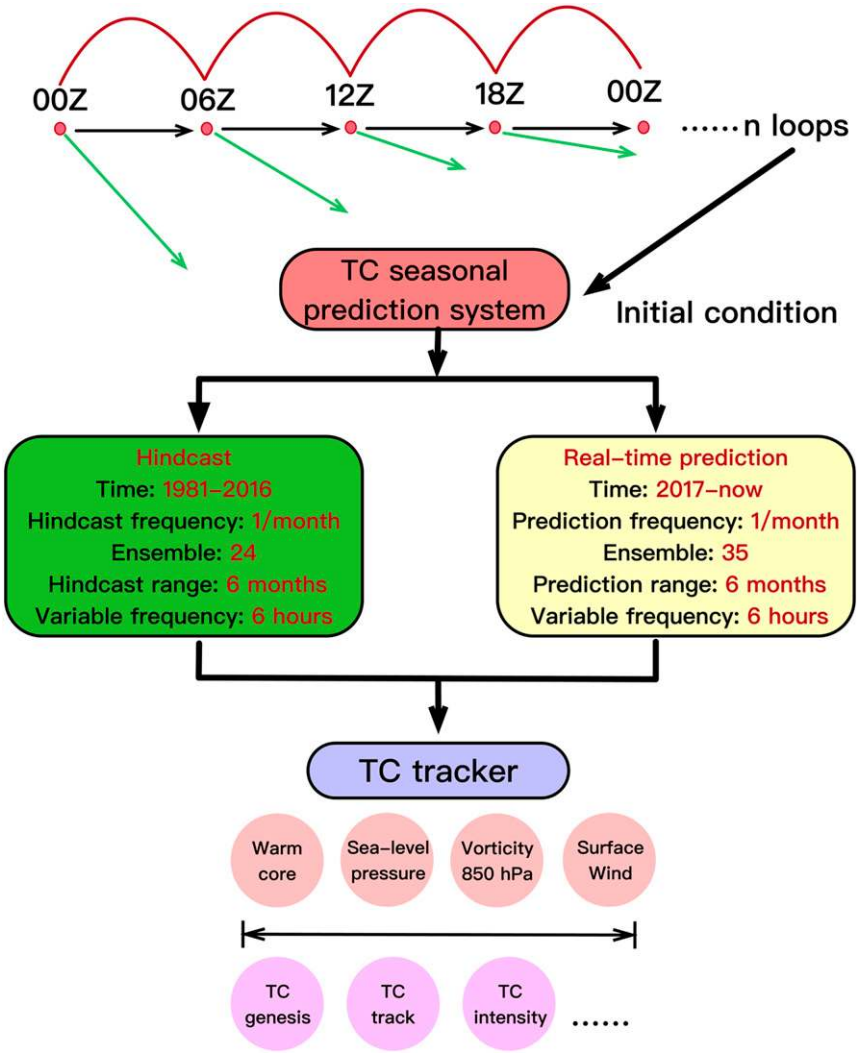

FIG. 1. Main structure of the dynamical TC seasonal prediction system, FGOALS-f2 V1.0, used in this study. A time-varying nudging method, which is based on the incremental analysis updating (IAU) process, is used to provide the initial conditions for the seasonal prediction. A total of 24 and 35 ensembles are used in the hindcast and real-time prediction framework, respectively. Variables at 6-h intervals (warm core, sea level pressure, 850-hPa vorticity, and surface wind) are used for TC detection, and the TC characteristics are diagnosed.

likelihood. The seasonal prediction of TCs mainly focuses on the seasonal anomalies of TC genesis, track density, intensity, and landfall. The results of TC seasonal forecasts mainly serve decision-makers in government, insurance and reinsurance companies, and other private sector entities. Compared with weather forecasts of particular individual storms, which are sensitive to the atmospheric initial conditions, the prediction signals for TCs on seasonal time scales mainly come from external forcings (e.g., greenhouse gases and aerosols), oceanic conditions (e.g., sea surface temperatures), land surface processes (e.g., soil moisture), and the large-scale air–sea pattern [e.g., the El Niño–Southern Oscillation (ENSO) and Madden–Julian oscillation (MJO)], in addition to the initial conditions (Camargo and Sobel 2005; Camargo et al. 2007b; Tang and Neelin 2004; Kim et al. 2009; Zhao et al. 2019; Camp et al. 2019; Moon et al. 2015).

Statistical methods were first applied to the seasonal prediction of TCs in the 1970s, due to the lack of computing resources, suitable resolution, and reasonable parameterization of physical processes for numerical models (Nicholls 1979; Gray 1984; Gray et al. 1993, 1994; Choi et al. 2014, 2016). These statistical seasonal prediction methods can be summarized into three steps: 1) find a statistical relationship between TC activity and a predictand; 2) develop a physical hypothesis for the observed statistical relationship; and 3) establish a statistical model that uses a single (or more often multiple) predictor(s)

to hindcast TC activity. For example, Gray et al. (1993, 1994) considered the effect of ENSO, African rainfall, Caribbean Sea level pressures and the quasi-biennial oscillation on TC activity and provided a seasonal prediction of TC activity in the North Atlantic (NA). Wang et al. (2013) used the western Pacific (WP) subtropical high as a critical predictor for the seasonal prediction of TCs in the Northwest Pacific. One of the advantages of statistical methods is that we can easily get a skillful prediction without the explicit physical connection between the large-scale factors and TCs. However, the disadvantage is that the physical relationships between the predictors and TCs might change with time (Nath et al. 2015; Zhang et al. 2016, 2017; Zhang and Villarini 2019), and overfitting in statistical methods can considerably reduce the accuracy of models.

The dynamical prediction skill for TCs in global climate models (GCMs) could be improved by increasing the horizontal resolution and improving physical parameterization processes. Wu and Lau (1992) used the Geophysical Fluid Dynamics Laboratory (GFDL) global general circulation model with a 417-km horizontal resolution to analyze TC activity and found that, as long as the large-scale pattern was reasonable in the model, it could capture TC-like structure. In recent years, analyzing TC activity using GCMs has become popular (Oouchi et al. 2006; Manganello et al. 2012, 2014; Murakami et al. 2012; Small et al. 2014). Zhao et al. (2019) evaluated the simulation performance of TCs in the GFDL High Resolution Atmospheric Model (HiRAM) with a 50-km horizontal resolution, and showed that it can reproduce the climatology and variability of TC activity reasonably in the WP and NA. Climate models have the ability to simulate many aspects of TC activity, and show potential in the prediction and projection of TC activity (Knutson et al. 2010; Vitart et al. 2003; Walsh et al. 2016; Camargo and Wing 2016; Baldwin et al. 2019). In addition, the climate models participating in the most recent phase of the Coupled Model Intercomparison Project (i.e., phase 6; CMIP6) (Eyring et al. 2016) can simulate TC activity with a 100-km resolution (Zhao et al. 2018a,b; Li et al. 2019).

Dynamical TC prediction on seasonal time scales began in the 1990s, and since that time the European Centre for Medium-Range Weather Forecasts (ECMWF) has started to make operational predictions of TCs on subseasonal-to-seasonal time scales (Vitart 2014; Manganello et al. 2016). The dynamical approach based on its model can provide spatial and temporal patterns that may better predict seasonal TC activity compared with traditional statistical regression methods. Chen and Lin (2013) applied HiRAM to make seasonal predictions of TCs with a fixed sea surface temperature (SST) and demonstrated high skill in retrospective seasonal forecasts of TCs in the WP ($r = 0.36$) and NA ($r = 0.89$). Murakami et al. (2016b) used the high-resolution GFDL coupled climate model HiFLOR to evaluate the prediction skill for major hurricanes and landfalling TCs, and found a positive contribution to TC prediction when increasing the horizontal resolution and accounting for air–sea interaction. Compared with regional models, the advantage of GCMs in TC prediction is that boundary effects are avoided, and there is no tuning required for a specific region, which is beneficial for extracting the predicted signal from the large-scale pattern (Mason et al. 1999; Chen et al. 2019a,b; Jia et al. 2015; Manganello et al. 2019; Zhou et al. 2019; Li et al. 2016; Davis and Zeng 2019). Murakami et al. (2016b) found that a high-resolution climate model could predict both NA seasonal TC numbers and landfalling TC numbers with skill ($r = 0.63$ for TC; $r = 0.69$ for hurricane). The latest generations of GCMs have the potential for TC prediction from synoptic to climatic time scales (Alessandri et al. 2011; Arribas et al. 2011; Murakami et al. 2015, 2016a,b; MacLachlan et al. 2015; Villarini et al. 2019). The Subseasonal to Seasonal Prediction (S2S) project based on a multimodel ensemble is an effective resource for reducing uncertainty in TC prediction (Vitart and Robertson 2018). The S2S project, which was approved by the World Meteorological Organization, was originally designed to provide a platform for models to provide forecasting information. Previous studies have shown that the S2S prediction skill for TCs is increased when more models are considered (Vitart and Robertson 2018; Vitart et al. 2017).

TABLE 1. The Saffir–Simpson hurricane wind scale (Simpson and Saffir 1974).

Category	Sustained winds (kt)
Tropical storm	34–63
1	64–82
2	83–95
3	96–112
4	113–136
5	≥137

In this study, using a fully coupled climate system model and a nudging-based initialization method, we first developed an ensemble seasonal prediction system, named FGOALS-f2 version 1.0 (Bao et al. 2018). The climate system model, named CAS FGOALS-f2 (He et al. 2019; Li et al. 2019; Bao and Li 2020) was developed by the State Key Laboratory of Numerical Modeling for Atmospheric Sciences and Geophysical Fluid Dynamics (LASG) at the Institute of Atmospheric Physics (IAP), which is part of the Chinese Academy of Sciences (CAS). Li et al. (2019) comprehensively evaluated the performance of TC activity in the atmospheric component of CAS FGOALS-f2 and found that the 1° model (horizontal resolution of 100 km) was able to successfully reproduce TC activity, including the climatological features and interannual variability. Wang et al. (2015) summarized recent progress in seasonal prediction research in China and pointed out that the seasonal prediction of TC activity in China is mainly based on statistical methods. Klotzbach et al. (2019) discussed the forecast methods, outputs and skill for several TC forecasting agencies around the world, and they found that both the hindcast and real-time prediction of TC activities in the WP and other TC basins have shown good skill. Therefore, the primary aim of this paper is to

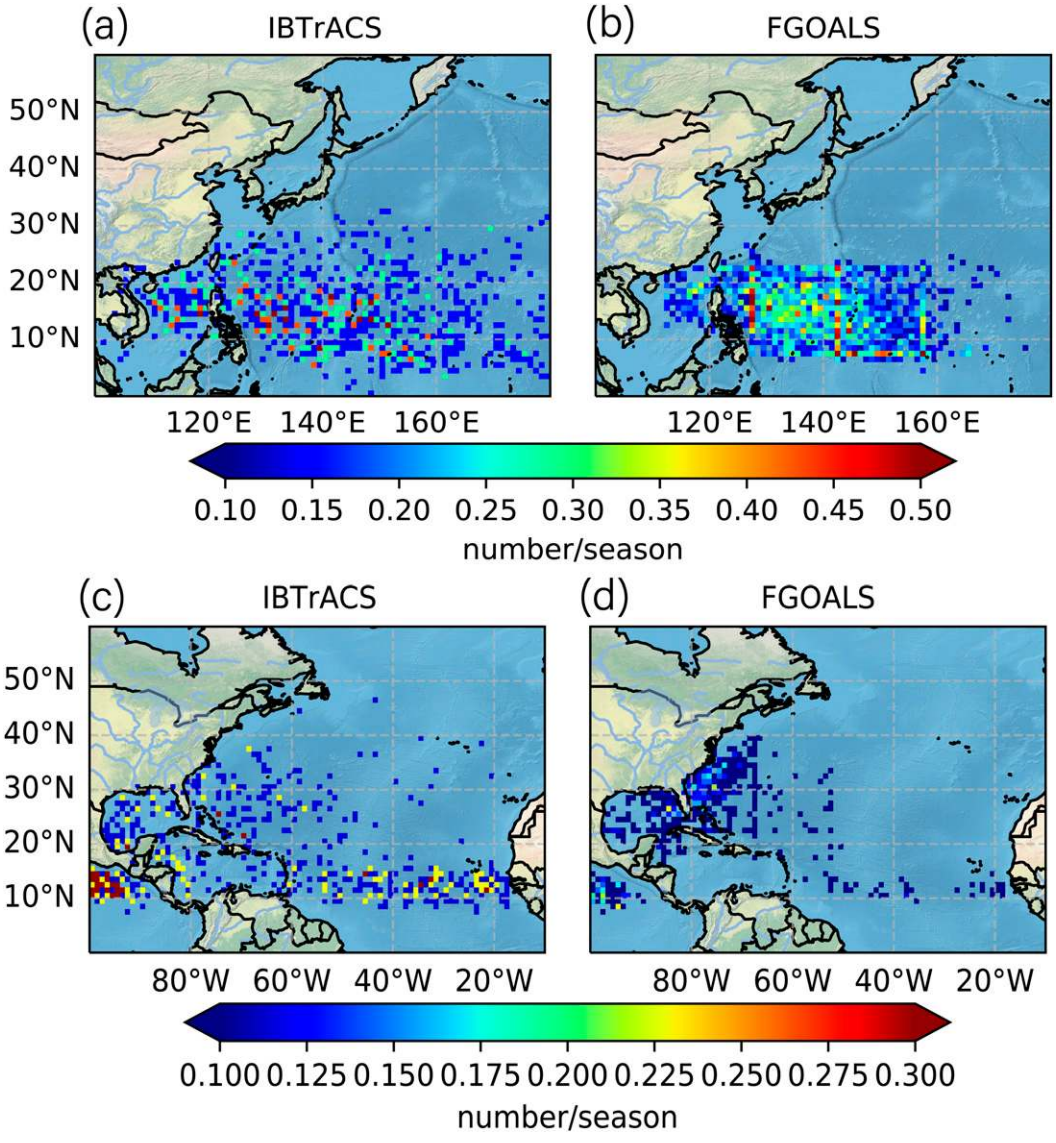

FIG. 2. (a),(b) The observed and FGOALS-forecast TC genesis location density for the WP, and (c),(d) the observed and FGOALS-forecast TC genesis location density for the NA. The TC density is analyzed in a $1° \times 1°$ grid box with 6-h intervals, and the unit of the color map is number per season (July–November). The 24-ensemble-member results of FGOALS-f2 V1.0 for the WP and NA in (b) and (d) are shown from 1981 to 2015. The IBTrACS data in the same period for the WP and NA in (a) and (c) are also shown as the observations.

evaluate the dynamical seasonal prediction skill for TCs in the WP and NA using FGOALS-f2 V1.0 and to determine how well a 1° dynamical prediction system can predict TC activity.

The remainder of this paper is organized as follows. Section 2 introduces the dynamical model and configuration of the seasonal prediction system. Section 3 introduces the observational dataset and the TC detection method. In section 4, the climatology and interannual variability of the predicted TC activity in the WP and NA are shown. The impact of ensemble sizes is discussed in section 5. The large-scale factors and the possible link between TC activity and ENSO on seasonal time scales are discussed in sections 6 and 7. In section 8, a recent 3-yr real-time forecast skill of TCs in the WP is given. In section 9, the monthly prediction skill of TCs is shown. Last, a brief discussion and summary of the results are given in section 10.

2. Dynamical model and seasonal prediction system

a. Climate system model (CAS FGOALS-f2)

There are four fully coupled components in the CAS FGOALS-f2 model: atmosphere, ocean, land, and sea ice. CAS

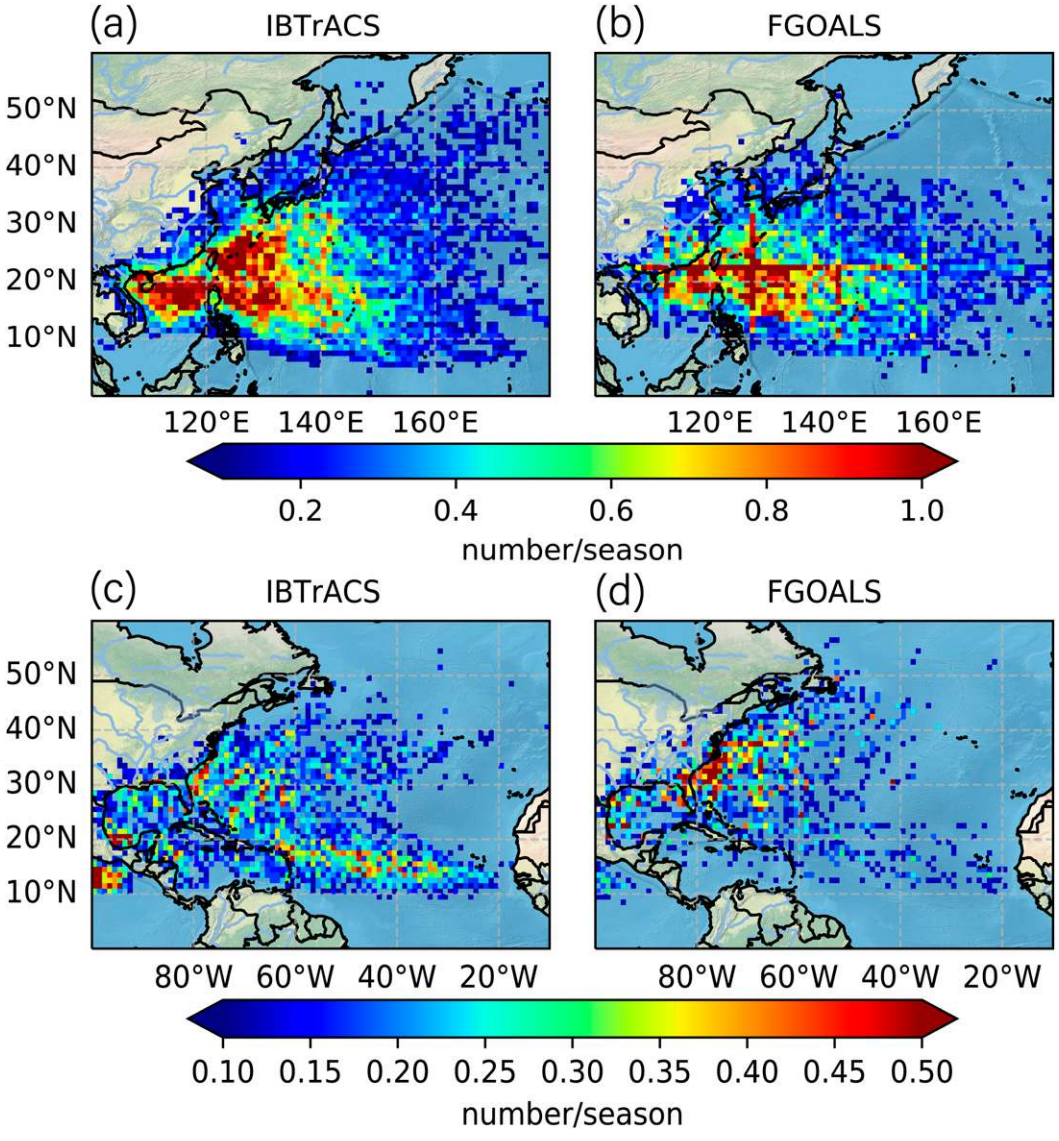

FIG. 3. As in Fig. 2, but for TC track density.

FGOALS-f2 has a standard horizontal resolution of 100 km. The atmospheric component of FGOALS-f2, FAMIL2, is the latest-generation atmospheric model of LASG/IAP/CAS. It uses a finite-volume method (Lin 2004) as the dynamical core, which is discretized on a cubed-sphere grid system (Putman and Lin 2007). The microphysics parameterization used in FGOALS-f2 is from GFDL (Zhou et al. 2019), and six species are considered. The cumulus parameterization used in FGOALS-f2 is a convection-resolving precipitation scheme (Bao and Li 2020), which involves calculating the microphysics in the cumulus processes for both deep and shallow convection. According to a previous evaluation, FAMIL2 showed stable computing performance on a supercomputer (Li et al. 2017; Zhou et al. 2012, 2015), and the simulation performance of TCs at C96 (horizontal resolution of approximately 100 km) has also been previously reported (Li et al. 2019). As the atmospheric component of FGOALS-f2, FAMIL2 has participated in CMIP6 activities (Eyring et al. 2016), the Global Monsoons Model Intercomparison Project (Zhou et al. 2016; He et al. 2019) and the High-Resolution Model Intercomparison Project (HighresMIP) (Haarsma et al. 2016; Bao et al. 2020). The land surface model used in FGOALS-f2 is version 4 of the Community Land Model (CLM4.0) (Oleson et al. 2010; Lawrence et al. 2011). The sea ice model and ocean model used in FGOALS-f2 are the Los Alamos Sea Ice Model, version 4.0 (CICE4.0) (Hunke et al. 2008), and the Parallel Ocean Program, version 2 (POP2) (Kerbyson and Jones 2005), respectively.

b. Dynamical seasonal prediction system FGOALS-f2 V1.0

Figure 1 shows the main structure of the dynamical TC seasonal prediction system based on FGOALS-f2 V1.0 in

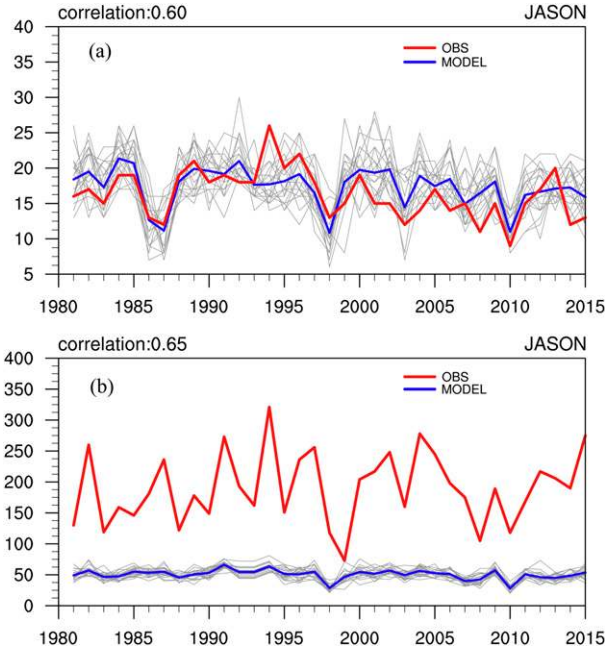

FIG. 4. Rank correlation between the IBTrACS and hindcasts of FGOALS-f2 V1.0 based on the track density of TCs. The 24-ensemble-member and 35-yr data are analyzed on a 1° × 1° grid box with 6-h intervals. Color shading indicates that the correlation coefficients are significant at a two-sided $P = 0.1$ level. The gray shading indicates the regions where the observed track density is nonzero for at least 25% of the years (approximately 9 years).

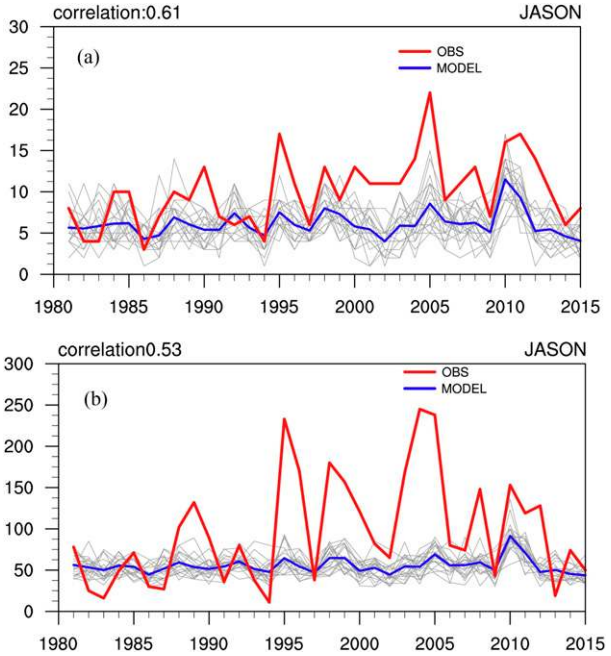

FIG. 5. (a) Hindcast of TC frequency and (b) ACE in the WP from July to November during 1981–2015. The red lines show IBTrACS, and the blue lines show the ensemble-mean hindcast of FGOALS-f2 V1.0. Each gray line indicates a single ensemble for the hindcast. The correlation coefficients between the observations and ensemble-mean hindcast of FGOALS-f2 V1.0 are also shown for each panel.

real-time prediction and hindcast conditions. To evaluate the seasonal prediction skill of TCs in FGOALS-f2 V1.0 systematically, a 35-yr hindcast (1981–2015) was designed with 24 ensemble members. Temperature, surface wind, surface pressure, and sea level pressure from the Japanese 55-year Reanalysis dataset (JRA55) (Kobayashi et al. 2015) were assimilated using a time-varying nudging method as the initial atmospheric conditions, which was based on the incremental analysis updating (IAU) process (Bloom et al. 1996). The relaxation factor within the time window of the assimilation varied with time (red curve in Fig. 1), and the biases between the simulation and reanalysis data were effectively limited to within a certain range with multiple assimilation loops. In the oceanic component, the potential temperature in the Global Ocean Data Assimilation System (GODAS) reanalysis data (Huang et al. 2010) was also nudged as the initial oceanic conditions. Although these data were not the initial conditions in the land surface and sea ice components of FGOALS-f2 V1.0, the initial conditions in the atmospheric and oceanic components drove the others to equilibrium.

The nudging time step was 6 h for the atmospheric component but with a slow nudging time step of 90 days for the oceanic component. A total of 24 ensemble members were generated for the hindcast based on a time-lag perturbation method. To obtain a stable integration, a 5-yr spinup time from 1976 to 1980 was adopted, for which the initial conditions of the ocean were derived from the historical run of FGOALS-f2. The real-time prediction of FGOALS-f2 V1.0 commenced in early 2017 (Bao et al. 2018). The only difference between the hindcast and real-time prediction was the ensemble size, which was increased from 24 to 35 for the real-time prediction. Each of the members in the hindcast and real-time prediction were integrated for up to 6 months, and the forecast frequency was once per month (on the 20th day of each month). Output data at 6-h intervals were used to diagnose TCs.

3. Observational data and TC detection method

a. *Observational data*

The International Best Track Archive for Climate Stewardship v03r10 (IBTrACS) (Knapp et al. 2010) was used for TC observational data. IBTrACS is a multisource dataset, and the data sources of IBTrACS used in this study were from the National Oceanic and Atmospheric Administration's (NOAA) National Hurricane Center for the North Atlantic and east Pacific (HURDAT2) (Landsea and Franklin 2013), the China Meteorological Administration for the west Pacific (Ying et al. 2014), and the Joint Typhoon Warning Center for the remainder of the globe (Chu et al. 2002). The time interval of the dataset is 6 h, which matches the model output. Manganello et al. (2012) pointed out that it is necessary to transform the 1-min-averaged maximum sustained winds to 10-min-averaged maximum sustained winds to provide a good platform to make comparisons between IBTrACS and the hindcast of FGOALS-f2 V1.0. In line with previous

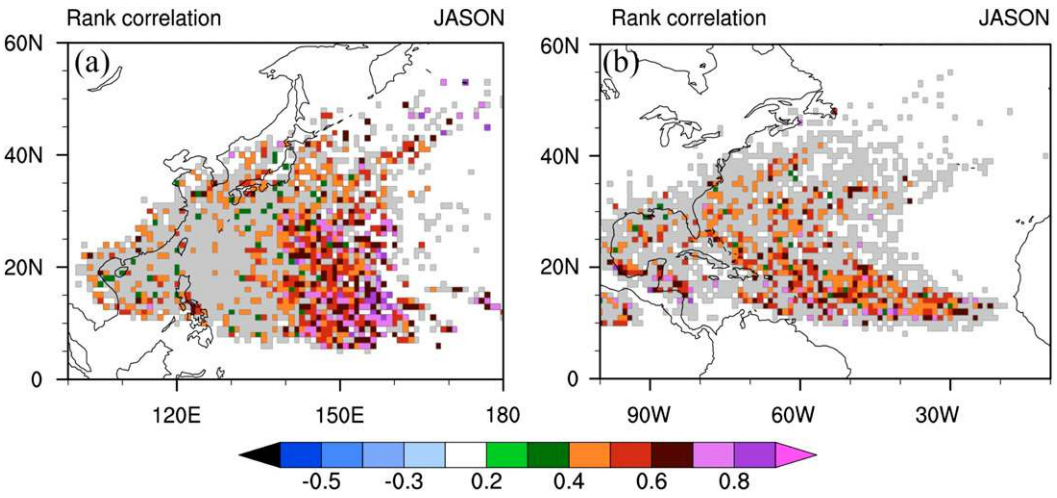

FIG. 6. As in Fig. 4, but for the NA.

studies (Manganello et al. 2012; Li et al. 2019), the coefficient was set to 0.88, which is based on a theoretical estimation (Knapp et al. 2010). This means that the threshold of a tropical storm is decreased from 18.01 to 15.84 m s^{-1}. The ERA-Interim data (ECMWF interim reanalysis) (Dee et al. 2011) and OISSTv2 (Optimum Interpolation Sea Surface Temperature, version 2) data (Banzon et al. 2016; Reynolds et al. 2007) for the period 1981–2015 were used to evaluate the large-scale atmospheric/oceanic conditions related to the TCs in FGOALS-f2 V1.0.

b. TC detection method

An objective feature-tracking approach was used to detect model-generated TCs based on the 6-h outputs of IBTrACS and the hindcast of FGOALS-f2 V1.0 (Fig. 1). We used the following fields to detect TCs: sea level pressure, warm core (average temperature anomaly between 300 and 500 hPa), 10-m wind, and 850-hPa vorticity. These fields are similar to the method used in the GFDL climate model (Zhao et al. 2009; Chen and Lin 2013; Xiang et al. 2015). Li et al. (2019) used this approach to evaluate the simulated performance of TCs in FAMIL2 and obtained reasonable results. The detection algorithm consists of three steps:

1) The local maximum 850-hPa absolute vorticity within a 600 × 600 km^2 grid box is defined as a potential TC. Then, there must be a minimum sea level pressure and a warm core (1°C warmer than the surroundings) within a 2° × 2° grid box centered on the 850-hPa absolute vorticity maximum. 2) The potential TCs are tracked and a judgment is made as to whether the potential TCs satisfy the following criteria: (i) TC lifetime > 72 h; (ii) surface wind > 17.4 m s^{-1}. 3) TCs are then classified based on the Saffir–Simpson hurricane wind scale (Simpson and Saffir 1974) (Table 1), and the TC genesis locations are divided into seven basins: north Indian Ocean, western North Pacific Ocean, eastern North Pacific Ocean, North Atlantic Ocean, south Indian Ocean, South Pacific Ocean, and South Atlantic Ocean. We use the same definition as IBTrACS for TC basin delineations.

4. Climatology and interannual variability of predicted TC activity in WP and NA

Figures 2a and 2b show the density of TC genesis locations (July to November) in the WP, as analyzed on a 1° × 1° grid box for IBTrACS and FGOALS-f2 V1.0. The initial time of prediction is 20 June during 1981–2015, and the ensemble-mean result is analyzed. Based on observations (Fig. 2a), there are two active regions for TC genesis location density. One of these active regions is in the South China Sea (SCS), and the other is over the WP east of the Philippines. We find that FGOALS-f2 V1.0 (Fig. 2b) captures the TC genesis

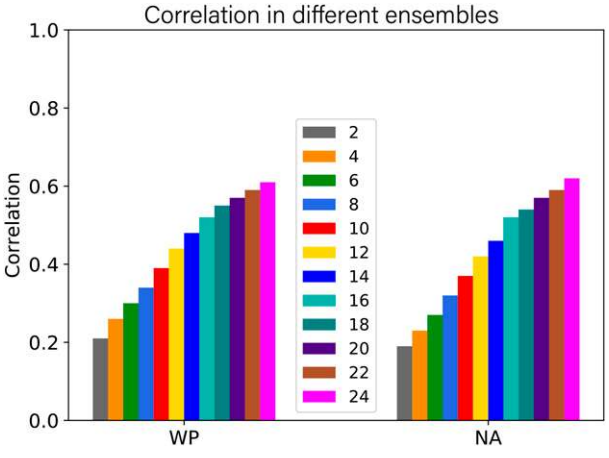

FIG. 7. Linear correlation coefficients of TC numbers between IBTrACS and the ensemble-mean hindcast of FGOALS-f2 V1.0 from July to November during 1981 to 2015. Different colors indicate the correlation coefficients for different ensemble sizes (2–24 members).

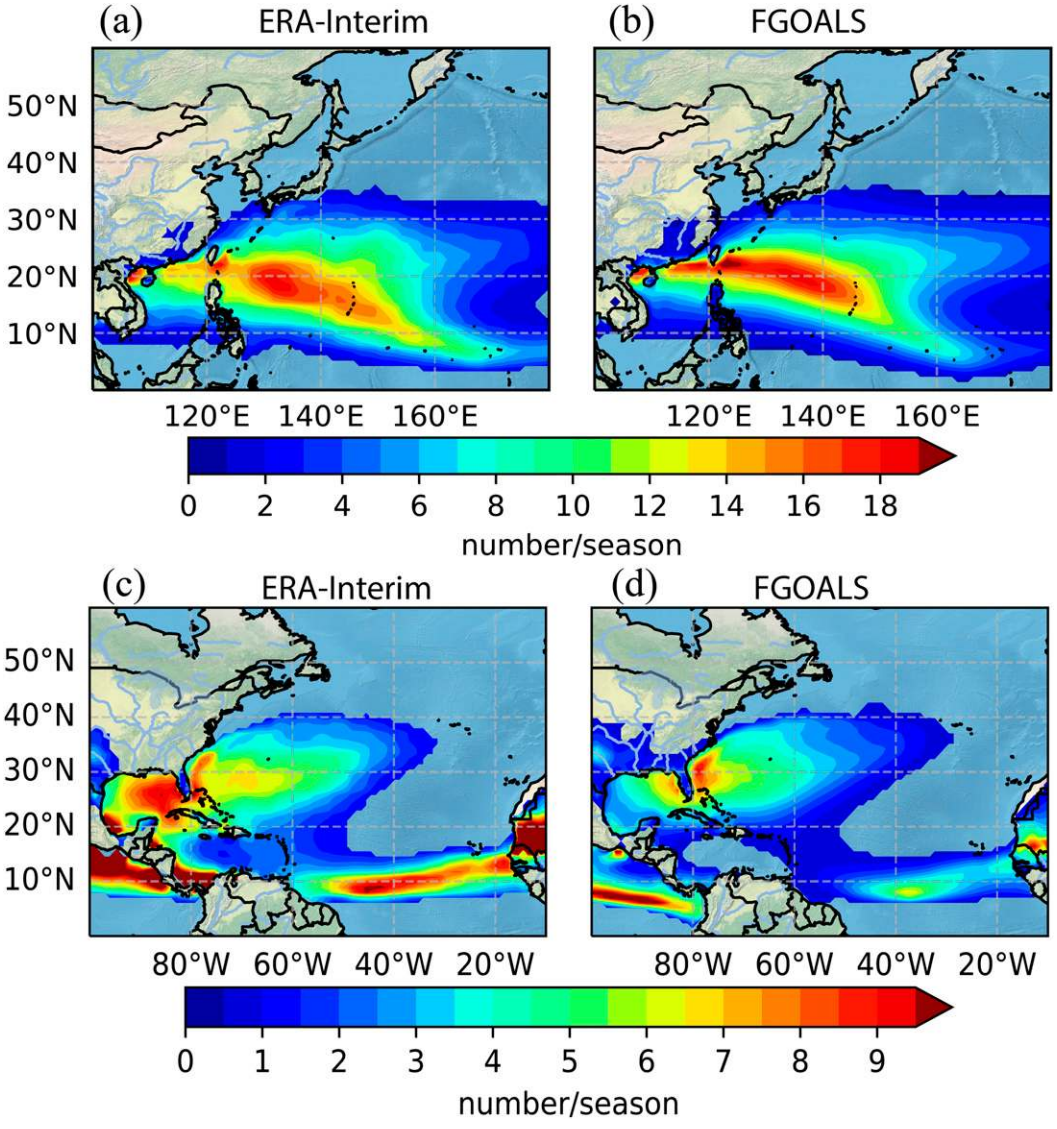

FIG. 8. TC GP index from July to November (JASON) during 1981–2015, based on the (a),(c) ERA-Interim reanalysis data and (b),(d) data of the FGOALS-f2 V1.0 hindcast. Both the GP index in the (top) WP and the (bottom) NA are shown.

location pattern, with the model correctly highlighting an active TC genesis region over the WP east of the Philippines. However, FGOALS-f2 V1.0 underestimates TC density in the SCS, reflecting the biases in the large-scale circulation (e.g., ENSO, MJO, and monsoon) in FGOALS-f2 V1.0 (Chan et al. 1998; Chen 2011). While similar active regions have been predicted in hindcasts of TC activity (May to November) in the ECMWF model (Manganello et al. 2016), which was initialized on 1 May, there was a northward shift of the TC genesis locations compared with IBTrACS. By comparison, there is no such bias in the WP TC genesis location for FGOALS-f2. The density of TC genesis locations in the NA is shown in Figs. 2c and 2d. Negative biases appear in the main development region compared with IBTrACS. The result is similar to a FAMIL2 simulation, which is the atmospheric component of FGOALS-f2, in an AMIP-like run (Li et al. 2019).

The densities of the TC tracks in IBTrACS and the hindcast of FGOALS-f2 V1.0 are shown in Figs. 3a and 3c for the WP and in Figs. 3b and 3d for the NA. There are more TCs to the northeast of the Philippines in the model than in the observations. Negative biases occur in the SCS, meaning that fewer TCs make landfall in Indochina compared with observations. This bias in TC tracks in the SCS are mainly due to fewer TCs forming in the SCS, which indicates that the medium resolution model is not enough to resolve TC activity in this region. The northeastward propagation of TCs in FGOALS-f2 V1.0 compares well with IBTrACS. The

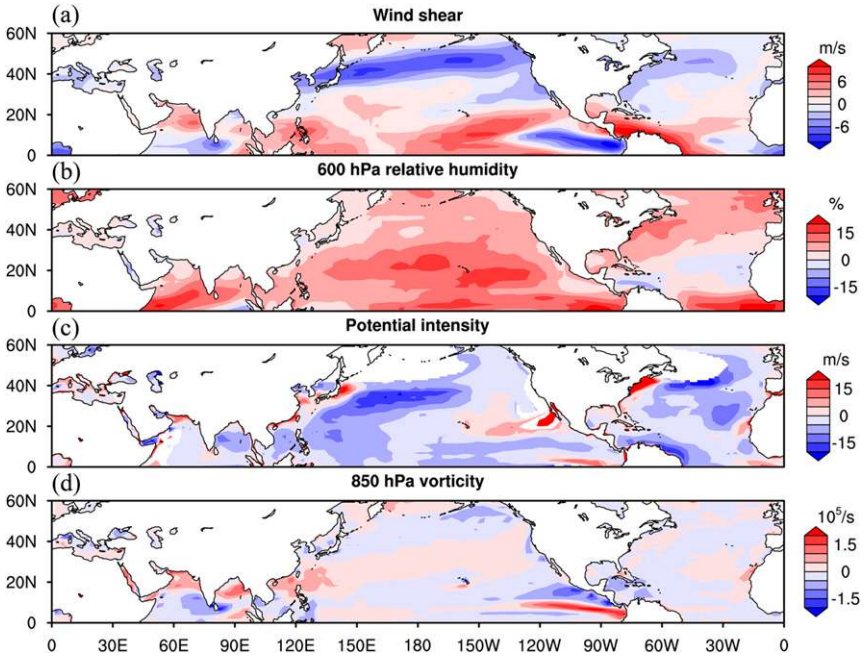

FIG. 9. Biases of the GP index component of TCs between ERA-Interim and the hindcast of FGOALS-f2 V1.0 from July to November (JASON) during 1981–2015. (a) The wind shear bias between 200 and 850 hPa. (b) The relative humidity bias at 600 hPa. (c) The potential intensity bias. (d) The absolute vorticity bias at 850 hPa.

hindcast of FGOALS-f2 V1.0 underestimates the density of TC tracks in the NA, particularly between 10° and 20°N. Manganello et al. (2016) compared the seasonal prediction skill for TCs in the NA and found a significant improvement in predicted TC tracks when the horizontal resolution was increased. These results have been verified in other seasonal prediction systems (Murakami et al. 2016b; MacLachlan et al. 2015). The active region of TC tracks in the NA near Florida in FGOALS-f2 V1.0 is comparable to that of IBTrACS, but TC tracks in the Caribbean Sea and Gulf of Mexico are underestimated compared with IBTrACS. The systematic underestimation of TC genesis in the Main Development Region contributed to the negative biases of TC tracks in these regions. On the other hand, the biases in the large-scale background flow led to more TCs moving northwest in FGOALS-f2 V1.0.

Next, we display the Spearman's rank correlation of TC track density, which is a widely used statistic to evaluate the prediction skill for TC tracks (Vecchi et al. 2014; Manganello et al. 2016; Murakami et al. 2016b), between the seasonal mean (July to November) of IBTrACS and the hindcast of FGOALS-f2 V1.0. Figure 4a shows the Spearman's rank correlation of track density in the WP. A high correlation coefficient is apparent in the TC generation region in the WP, but there is a low correlation coefficient in the primary TC development region (120°–130°E, 10°–25°N), which seems to be a common problem among prediction systems (Manganello et al. 2016; Murakami et al. 2016b). In addition, $r > 0.4$ in the SCS and near Japan, indicating the potential for the seasonal prediction of landfalling TCs. Weak correlation coefficients appear in the NA (Fig. 4b) compared with other seasonal prediction systems, mainly due to the negative biases that appear in FGOALS-f2 V1.0. Li et al. (2019) found that the negative biases of TC number in NA could be improved when increasing the horizontal resolution.

The interannual variability of TC number and accumulated cyclone energy (ACE) are shown in Figs. 5 and 6. ACE is a measure used to calculate the approximate energy over the lifetime of a TC when the one-minute maximum sustained winds are equal to or greater than 34 kt (1 kt $\approx$ 0.51 m s^{-1}).

Thus:

$$\mathrm{ACE} = 10^{-4}\sum v_m^2, \tag{1}$$

where v_m is the estimated sustained wind speed in knots.

We find a high correlation ($r = 0.60$) between predicted and observed TC numbers (July–November) in the WP (Fig. 5a). There is a significant correlation between WP TC numbers and ENSO according to IBTrACS, and the predicted TC numbers from the model show a similar response. The correlation of WP ACE between predicted and observed numbers (July to November) is 0.65 (Fig. 5b). However, underestimated values for the hindcast are found in years when typhoons were generated. These results mean that the prediction system does not do a good job of replicating typhoons. Although the correlation coefficient of TC numbers between observations and the hindcast in

the NA is high (Fig. 6a), the mean value and amplitude in the hindcast are weak compared with IBTrACS. Since the model has a negative bias in TC number and intensity in the NA, the correlation coefficient of TC ACE (Fig. 6b) is lower than it is in the seasonal prediction system in GFDL (Murakami et al. 2016b) and ECMWF (Manganello et al. 2016), where ACE correlations from May initializations are 0.61 and 0.82, respectively. It is worth noting that FGOALS-f2 configured with 100-km horizontal resolution cannot reproduce those years when TC activity was high over the WP and NA, especially in years when strong TCs occurred frequently. For example, FGOALS-f2 V1.0 underestimates the TC ACE by 80% in years when strong TCs occurred frequently (i.e., 1990. 1995, 1998, and 2005). Although the sign of the anomalies is correct, these underestimations of TC activity in FGOALS-f2 V1.0 affect the predicted value of both the real-time TC number and ACE (Fig. A1 in the appendix). Thus, there is still room for improvement in terms of real-time TC prediction skill of FGOALS-f2 when considering statistical methods and improving model resolution (Murakami et al. 2016a,b). For example, scale ACE from the model to make it match more with observations.

5. Impacts of the ensemble members

Ensemble prediction schemes are useful for improving seasonal prediction skill of TC activity. Manganello et al. (2016) found that linear correlations between May to November observed (IBTrACS) and predicted TC frequencies increased and errors have decreased when the ensemble sizes were increased from 1 to 51. FGOALS-f2 used 24 ensembles for hindcasts and 35 ensembles for real-time prediction. The sensitivity of the prediction skill to the ensemble size in the hindcast of FGOALS-f2 V1.0 is shown in Fig. 7. The correlation coefficient increases when the ensemble size is increased from 2 to 24. Even using all 24 ensemble members, the prediction skill of the model does not look to be saturated. The ECMWF's TC prediction system uses 51 ensemble members for seasonal prediction, which is the maximum threshold for the growth of prediction skill according to Manganello et al. (2016). We increased the ensemble members from 24 to 35 to improve TC prediction skill in real time. This approach has been operationally used in the China Multi-Model Ensemble Prediction System V1.0 (CMMEv1.0) (Ren et al. 2019), but the computing cost of the prediction is a constraint for increasing ensemble members. On the other hand, it should be noted that the increasing trend of the correlation coefficient is not linear, and the skill tends to saturate for the current initialization method in FGOALS-f2 V1.0 (Manganello et al. 2016; Chakraborty et al. 2020).

6. Genesis potential index and large-scale parameters

We used the genesis potential (GP) index from Emanuel and Nolan (2004) to investigate the contributions of specific environmental variables to the genesis of TCs. Camargo et al. (2007b) used the GP index to diagnose ENSO effects

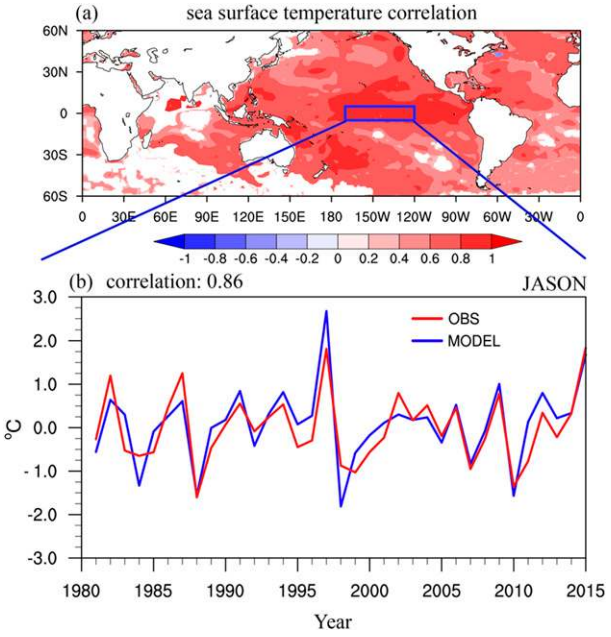

FIG. 10. (a) Correlation coefficients of SST between the hindcast of FGOALS-f2 V1.0 and OISSTv2 from July to November during 1981–2015, for which the values at the 95% confidence level are shown. (b) Correlation of the Niño-3.4 index, highlighted with the blue rectangle in (a), between FGOALS-f2 V1.0 and OISSTv2.

on TC activity, and found that the GP index succesfully reproduces the climatology and variability of TC activity compared with the observations. The GP index used in this study is defined as follows:

$$\mathrm{GP} = |10^5 \mathrm{Vort}_{850}|^{3/2} \left(\frac{\mathrm{RH}}{50}\right) \left(\frac{V_m}{70}\right) (1 + 0.1 V_{\mathrm{shear}}), \qquad (2)$$

where Vort_{850} is the 850-hPa absolute vorticity (s^{-1}), RH is the 600-hPa relative humidity (%), V_m is the maximum potential intensity (Emanuel 1995; Emanuel and Sobel 2013), and V_{shear} is the magnitude of the wind shear between 850 and 200 hPa ($\mathrm{m\,s}^{-1}$). Furthermore, the V_m (the maximum potential intensity) used in this paper is defined as follows:

$$V_m = \frac{C_k T_s}{C_d T_0} (\mathrm{CAPE}^* - \mathrm{CAPE}^b), \qquad (3)$$

where C_k is the exchange coefficient of enthalpy, C_d is the drag coefficient, T_s is the SST, and T_0 is the mean outflow temperature. CAPE^* is the convective available potential energy (CAPE) of the air lifted from saturation at sea level, and CAPE^b is the CAPE of the boundary layer air.

Figure 8 shows the GP index calculated from ERA-Interim data (Figs. 8a,c) and the FGOALS-f2 V1.0 hindcasts (Figs. 8b,d) from July to November for the WP and NA, respectively, during 1981–2015. In the WP, FGOALS-f2 V1.0 reproduces the pattern of the GP index, consistent with the results using

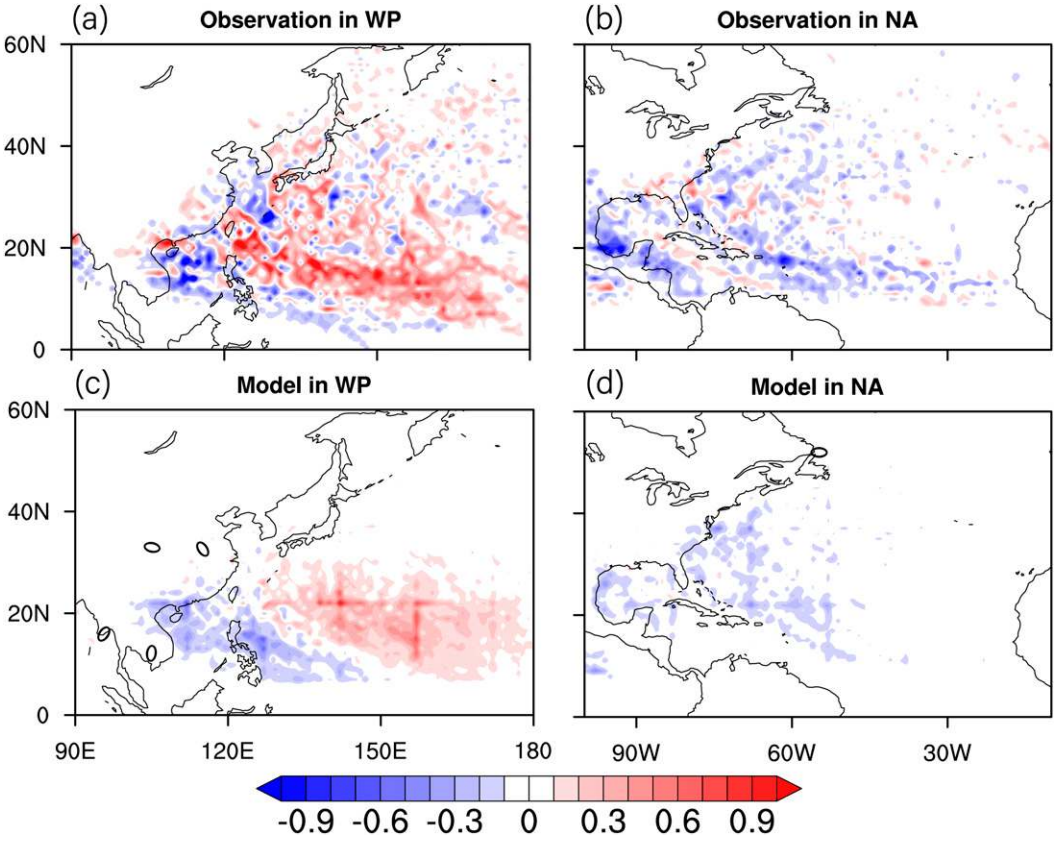

FIG. 11. Seasonal mean (July–November) track density of the TC difference between El Niño and La Niña years for (a),(b) OISSTv2 and (c),(d) the hindcast of FGOALS-f2 V1.0 in the (left) WP and (right) NA. El Niño years used in this figure are 1982, 1986, 1987, 1991, 1994, 1997, 2002, 2004, 2006, 2009, and 2015; La Niña years used in this figure are 1983, 1984, 1988, 1995, 1998, 1999, 2000, 2007, 2010, and 2011. Blue (red) anomalies show a negative (positive) El Niño effect.

the TC detection method. A negative bias appears in the NA, which reflects the bias of the large-scale pattern in FGOALS-f2 V1.0. Next, we display the differences in wind shear (Fig. 9a), 600-hPa relative humidity (Fig. 9b), potential intensity (Fig. 9c), and 850-hPa vorticity (Fig. 9d) between ERA-Interim and the hindcast of FGOALS-f2 V1.0 to highlight the error sources that contribute to the GP index. Positive wind shear biases appear in the NA, which is unfavorable for the formation of TCs in these basins. The systematic positive bias of 600-hPa relative humidity reflects vigorous evaporation in the surface layer, and this anomalously high level of water vapor reaches the middle troposphere with convective activity, consistent with previous studies (Wang et al. 2019a,b). Camargo et al. (2007b) found that vertical wind shear and midlevel relative humidity are important for TC formation, and the increase in relative humidity provides a more favorable environment for TC development. In addition, the negative biases of potential intensity and 850-hPa vorticity in the WP and NA reflect the negative biases of TC number and TC intensity in FGOALS-f2 V1.0. On the other hand, Camargo et al. (2020) found that there is no specific association between a conducive environment and TC activity in low-resolution models, and the relationship between the models' TC characteristics and environmental characteristics is strengthened when the model's resolution is increased.

7. Response of ENSO

There are many studies that have focused on the relationship between ENSO and TC activity in the WP and the NA (Wang and Chan 2002; Tang and Neelin 2004; Camargo and Sobel 2005; Kim et al. 2009; Domeisen et al. 2015). Wu and Lau (1992) used a coupled GCM from GFDL to discuss the relationship between ENSO and TC activity, but the significance of their results was not tested. They found a below-normal frequency of TCs in the WP in El Niño years, and more TCs occurred in the western South Pacific and western NA in La Niña years. Figure 10a shows the correlation between predicted and observed global SST from 1981 to 2015 (July to November). High correlation coefficients appear in both the WP and NA, which is likely one of the reasons why both basins have significant seasonal TC prediction skill. Furthermore, the correlation of the Niño-3.4 index between the predictions and

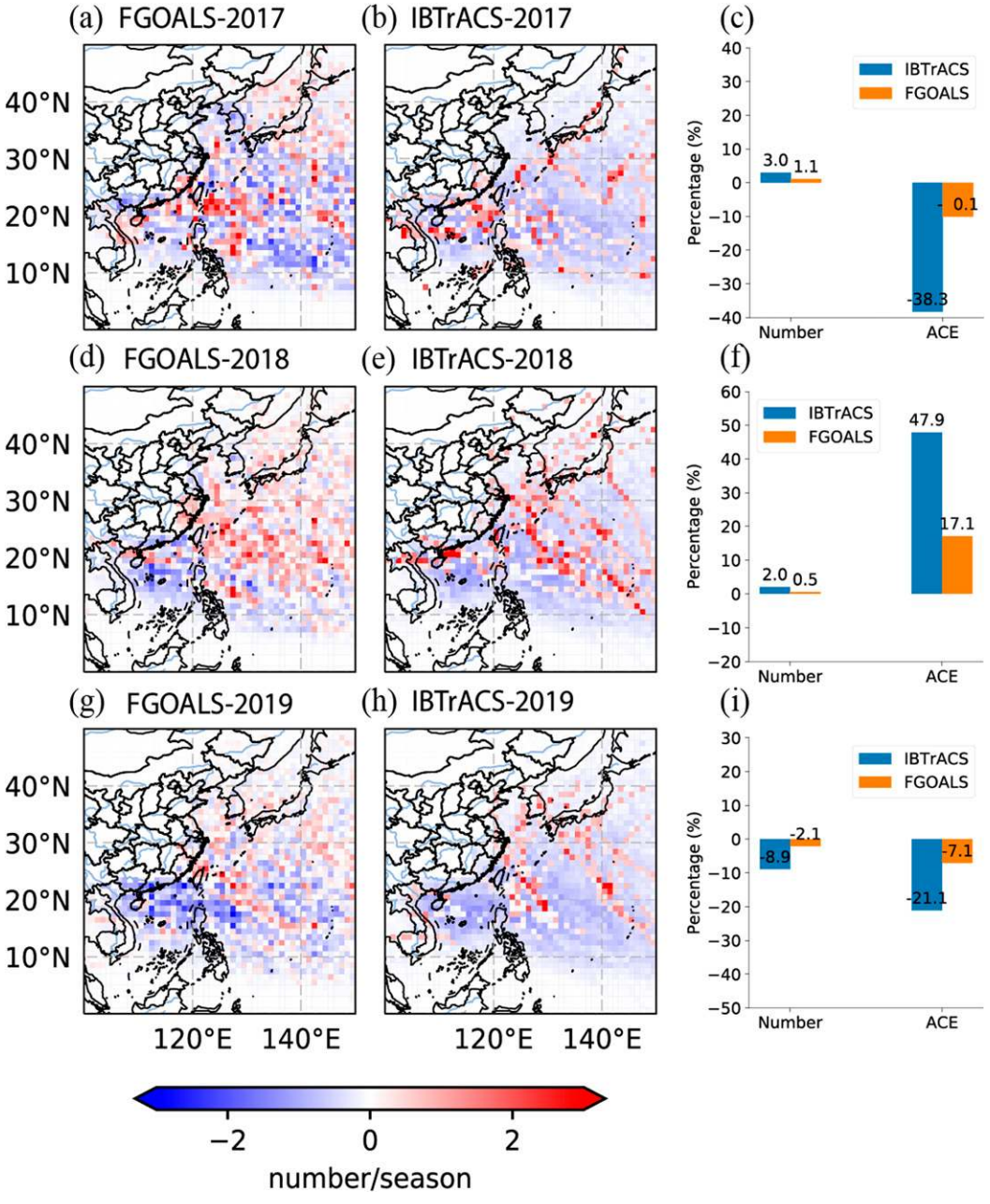

FIG. 12. Seasonal anomaly (July–November) of TC track density in the WP from 2017 to 2019 (unit: number per season). The TC density is analyzed in a 1° × 1° grid box with 6-h intervals, and the unit of the color map is number per season (July–November). (a),(d),(g) The 35-ensemble-member mean results of FGOALS-f2 V1.0 in the WP, and (b),(e),(h) the IBTrACS observations. (c),(f),(i) The anomaly percentage (%) of TC numbers and ACE for the entire WP basin from 2017 to 2019.

OISST is 0.86 (Fig. 10b), which reflecting a robust ENSO response in FGOALS-f2 V1.0.

Figure 11 shows the difference in track density between El Niño and La Niña years during 1981–2015 (Camp et al. 2015; Vecchi et al. 2014; Manganello et al. 2016; Shaevitz et al. 2014). We used the same ENSO definition as Camp et al. (2015)—that is, El Niño and La Niña years are defined by the average SST (August–October) anomaly being greater than 0.5°C and less than −0.5°C in the Niño-3.4 region, respectively. There are 11 El Niño years (1982, 1986, 1987, 1991, 1994, 1997, 2002, 2004, 2006, 2009, and 2015) and 10 La Niña years (1983, 1984, 1988, 1995, 1998, 1999, 2000, 2007, 2010, and 2011) using this definition in the hindcasts of FGOALS-f2 V1.0. Over the WP, observed TC activity increases east of the Philippines,

TABLE 2. Seasonal anomalies (July–November) of landfalling TCs in the provinces of China from 2017 to 2019 (%).

Province	2017: FGOALS/Obs	2018: FGOALS/Obs	2019: FGOALS/Obs
Hainan	23%/−33%	25%/42%	−24%/−33%
Guangxi	−25%/−30%	12%/26%	43%/−30%
Guangdong	21%/30%	−31%/−38%	−40%/−30%
Fujian	30%/53%	26%/20%	−15%/25%
Zhejiang	−22%/−34%	13%/30%	−12%/43%
Jiangsu	−22%/−34%	11%/50%	25%/46%

while it is reduced in the SCS when strong El Niño events occur (Fig. 11a). In the NA, observed TC activity decreases when strong El Niño events occur (Fig. 11b). These phenomena are captured well by FGOALS-f2 V1.0. While the effects of lifetime, intensity, and frequency all contribute significantly to the ENSO signal in ACE, there is a more significant correlation between TC ACE and ENSO in the WP compared to that between TC number and ENSO. One possible reason for this result is that there is a shift within the basin in the specific region of TC activity, which is modulated by the large-scale environment. ACE generally increases in the WP in El Niño year is due to TC formations shifting eastward and southward, leading to longer storm lifetimes and likely overall higher storm intensities (Camargo and Sobel 2005).

8. Real-time seasonal prediction of TCs

Real-time seasonal prediction of TC activity is still a challenge, but is of scientific value and is also a reference for disaster prevention and mitigation. A number of international modeling centers have begun real-time seasonal prediction of TC activity (Vitart and Robertson 2018; Murakami et al. 2018; MacLachlan et al. 2015; Klotzbach et al. 2019). However, dynamical seasonal prediction of TCs is still in its early stages (Wang et al. 2015). From 2017, FGOALS-f2 V1.0 began carrying out real-time seasonal prediction of TCs in the WP. The prediction ensemble size was increased from 24 to 35 from the hindcasts to the forecasts. Figure 12 shows the seasonal anomalies (July–November) of track densities in the WP from 2017 to 2019. Observed TC activity from July to November 2017 (Fig. 12b) is less than the climatology, and TC activity in the SCS is more frequent than it is at higher latitudes. By contrast, TC activity from July to November 2018 (Fig. 12e) is more frequent at higher latitudes. The pattern of track densities from July to November 2019 (Fig. 12h) is similar to what it is in 2018 (Fig. 12e), but 2018 TC activity in the SCS is more frequent than it is in July to November 2019. The ensemble-mean prediction of TC activity patterns in FGOALS-f2 V1.0 (Figs. 12a,d,g) are similar to the results of IBTrACS. In addition, the predicted anomaly percentage of TC numbers and ACE in the WP is reasonable compared to IBTrACS. However, the amplitude of the ACE in FGOALS-f2 V1.0 is smaller than it is in IBTrACS. Similar results for seasonal prediction of TCs in the NA are shown in Fig. A1. Furthermore, the percentage anomalies of landfalling TC numbers in the provinces of China are shown in Table 2. Predictions were of better quality for Guangdong and Jiangsu, while the worst prediction was for Hainan. However, it is worth noting that it is hard to make any comments about definitive model skill (or lack of skill) based off of just three years of data, especially for regional forecasts.

9. Monthly prediction of TCs

Figure 13 shows the one-to-three-month lead correlations for the monthly (July–November) TC numbers between IBTrACS and the hindcast of FGOALS-f2 V1.0 in the WP. Correlations improve with decreasing prediction interval, reflecting the potential for the prediction system to make skillful subseasonal TC predictions for the WP. The monthly rank correlation of track density (July–October) between IBTrACS and the hindcast of FGOALS-f2 V1.0 is shown in Fig. 14. High correlations appear in the areas where most TC genesis, and correlations for landfalling TCs also increase. The same results for monthly prediction

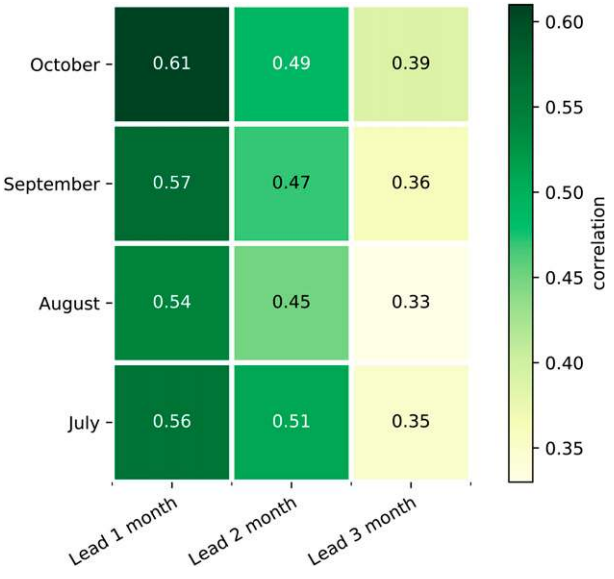

FIG. 13. Linear correlation coefficients of monthly TC frequency between IBTrACS and the ensemble-mean hindcast of FGOALS-f2 V1.0 from 1981 to 2015. The colors in the heat map are the correlation coefficients for a 1–3-month lead time for July–October.

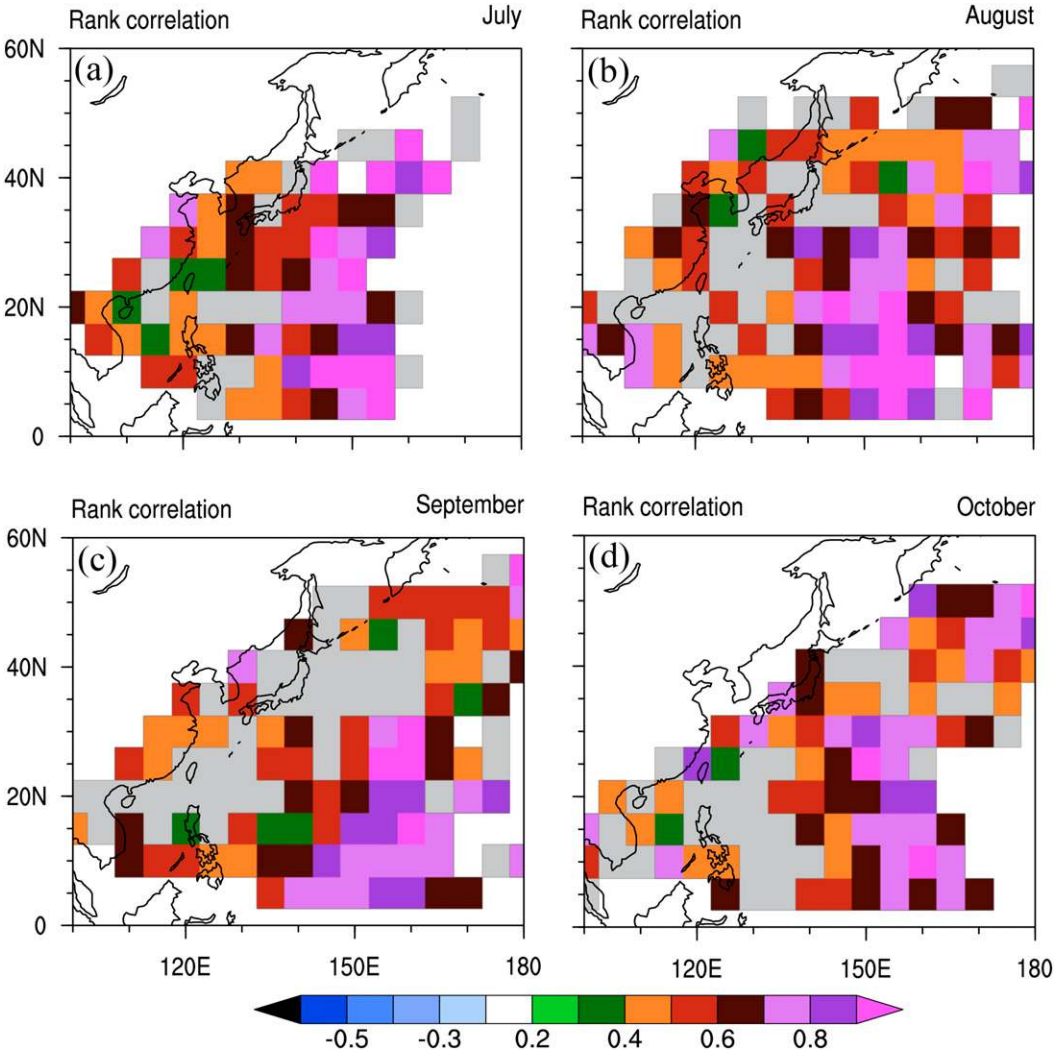

FIG. 14. Monthly (July–October) rank correlations between IBTrACS and the hindcast of FGOALS-f2 V1.0 in the WP based on the track density of TCs. The 24-ensemble-member and 35-yr data are analyzed in a 5° × 5° grid box with 6-h intervals. Color shading indicates that the correlation coefficients are significant at a two-sided $P = 0.1$ level. The gray shading indicates the regions where the observed track density is nonzero for at least 25% of the years (approximately 9 years).

of NA TC activity are shown in Figs. A2 and A3. In the future, the next generation of the dynamical prediction system from CAS/IAP/LASG will make daily ensemble predictions, and the results will be uploaded to the S2S project (Vitart and Robertson 2018; Vitart et al. 2017). In addition, the prediction skill for TC activity on subseasonal time scales (Camp et al. 2018, 2019; Gao et al. 2019) will be more fully evaluated in the future.

10. Summary and conclusions

A dynamical seasonal prediction system, FGOALS-f2 V1.0, was developed by CAS/IAP/LASG based on the FGOALS-f2 climate system model. A 35-yr hindcast with 24 ensemble members was used to evaluate the seasonal prediction skill for TC activity in the WP and NA. The hindcast TC prediction are initialized from 20 June, and the target season is from July to November, which is the climatological peak period for TC activity. Li et al. (2019) evaluated the simulation performance of TC activity in FAMIL2 (100-km horizontal resolution), which is the atmospheric component of CAS FGOALS-f3 (He et al. 2019), and the results from that study indicated that FAMIL2 can reasonably reproduce the genesis locations, tracks, and numbers of TCs. Thus, the indication is that the model can capture TC signals at a medium horizontal resolution scale (100 km) (Zhao et al. 2018a). The advantages of using a medium horizontal resolution scale are the smaller computational expense and the larger number of ensemble members compared with high-resolution model.

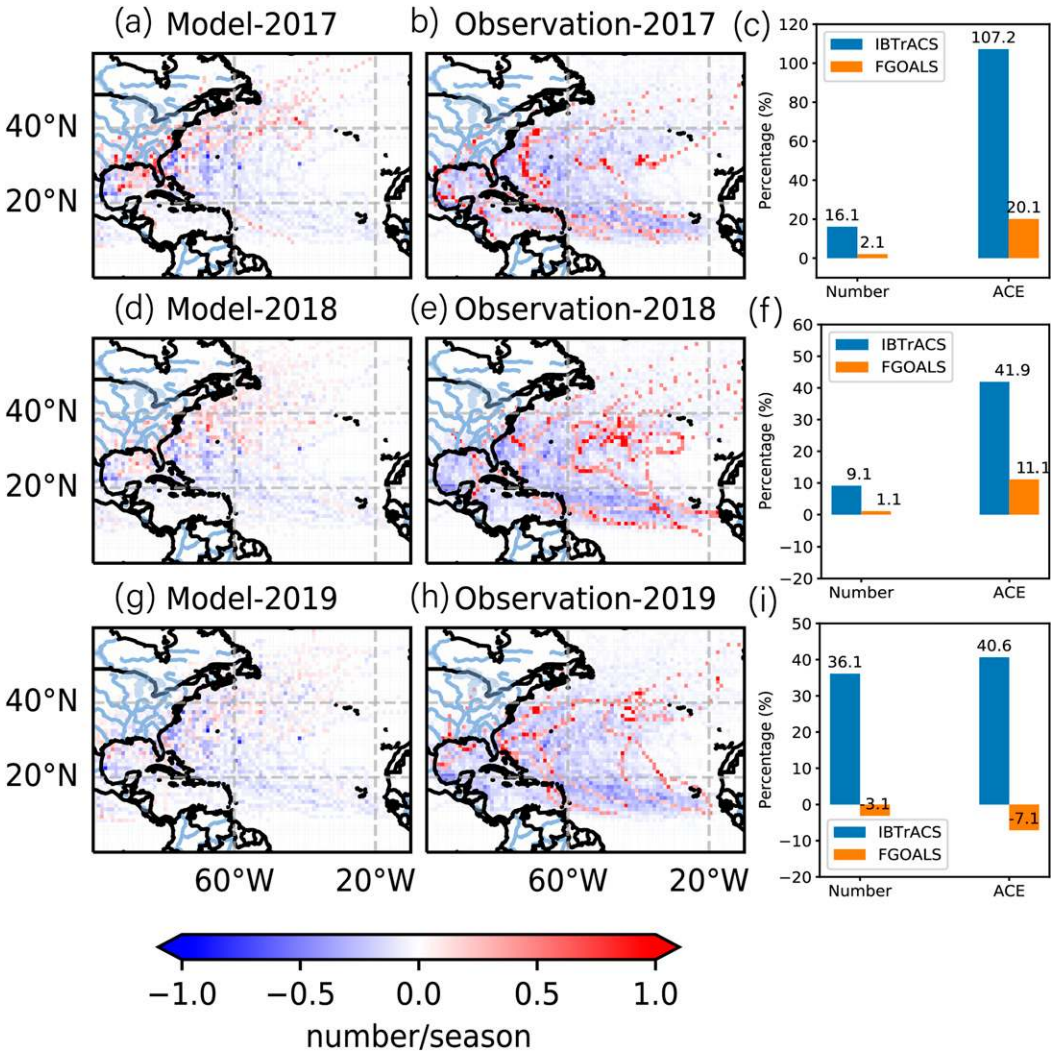

FIG. A1. As in Fig. 12, but for the NA.

In summary, FGOALS-f2 V1.0 can reproduce the seasonal (July–November) density of TC genesis locations and tracks in the WP, but underestimates the seasonal density of TC locations and tracks in the NA. The correlation between observed TC numbers and model hindcasts is 0.60 (significant at the 95% level) and 0.61 (significant at the 95% level) in the WP and the NA, respectively. However, the correlation coefficients of ACE are lower than those reported in other studies (Manganello et al. 2016; Camp et al. 2015; Murakami et al. 2018), reflecting the negative bias of predicted TC intensity in FGOALS-f2 V1.0. Strachan et al. (2013) discussed the advantages of increased horizontal resolution when simulating TCs, and they found a distinct positive correlation between horizontal resolution and the simulated intensity of TCs. We find that increasing the number of ensemble members helps to improve the seasonal prediction skill for TCs. The model's ability to represent both ENSO and its associated modulation of the GP index contributes to the seasonal prediction skill for TC activity in the WP and the NA. Also, FGOALS-f2 V1.0 shows skillful real-time seasonal prediction skill for TC numbers, tracks, ACE, and landfalling TCs in China during 2017–19. FGOALS-f2 V1.0 shows a considerable monthly prediction skill for TCs in the WP and NA.

In the future, we intend to increase the horizontal resolution in FGOALS-f2 V1.0 from 100 to 25 km, consistent with FGOALS-f3-H in HighresMIP (Bao et al. 2020). Murakami and Sugi (2010) found that the intensities, interannual variability, and seasonal cycle of simulated TCs could be improved when their model's horizontal rsolution was increased from TL95 (180-km mesh) to TL959 (20-km mesh). Given other modeling centers' improvements in TC prediction using higher resolutions, we believe that we too will find similar improvements in skill.

Acknowledgments. The research presented in this paper was jointly funded by the Strategic Priority Research Program of

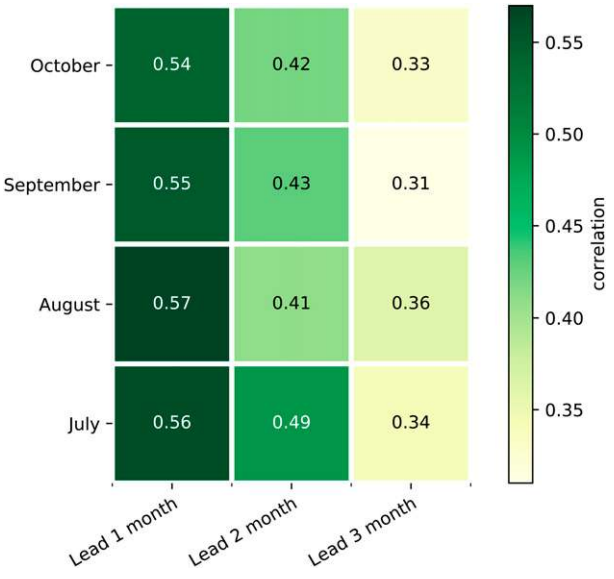

FIG. A2. As in Fig. 13, but for the NA.

the Chinese Academy of Sciences (Grant XDB40030205), the National Natural Science Foundation of China (Grants 91737306, 42005117, 41675100, and U1811464), and the Key Special Project for the Introducing Talents Team of the Southern Marine Science and Engineering Guangdong Laboratory (Guangdong) (Grant GML2019ZD0601).

Data availability statement. The IBTrACS data used in this study can be obtained from https://www.ncdc.noaa.gov/ibtracs/; the OISSTv2 data can be obtained from https://psl.noaa.gov/data/gridded/data.noaa.oisst.v2.highres.html; the ERA-Interim data can be obtained from https://www.ecmwf.int/en/forecasts/datasets/reanalysis-datasets/era-interim; and the hindcast and real-time output of FGOALS-f2 V1.0 are available by contacting the corresponding author.

APPENDIX

Prediction Skill of TC in NA

a. Real-time seasonal prediction of TCs in the NA

The seasonal anomaly (July–November) of track density in the NA from 2017 to 2019 (Fig. A1).

b. Monthly prediction of TCs in the NA

Figure A2 shows the 1–3-month leading correlation coefficients of the monthly (July–November) TC numbers between IBTrACS and the hindcast of FGOALS-f2 V1.0 in the NA. The monthly rank correlation of track density (July–October)

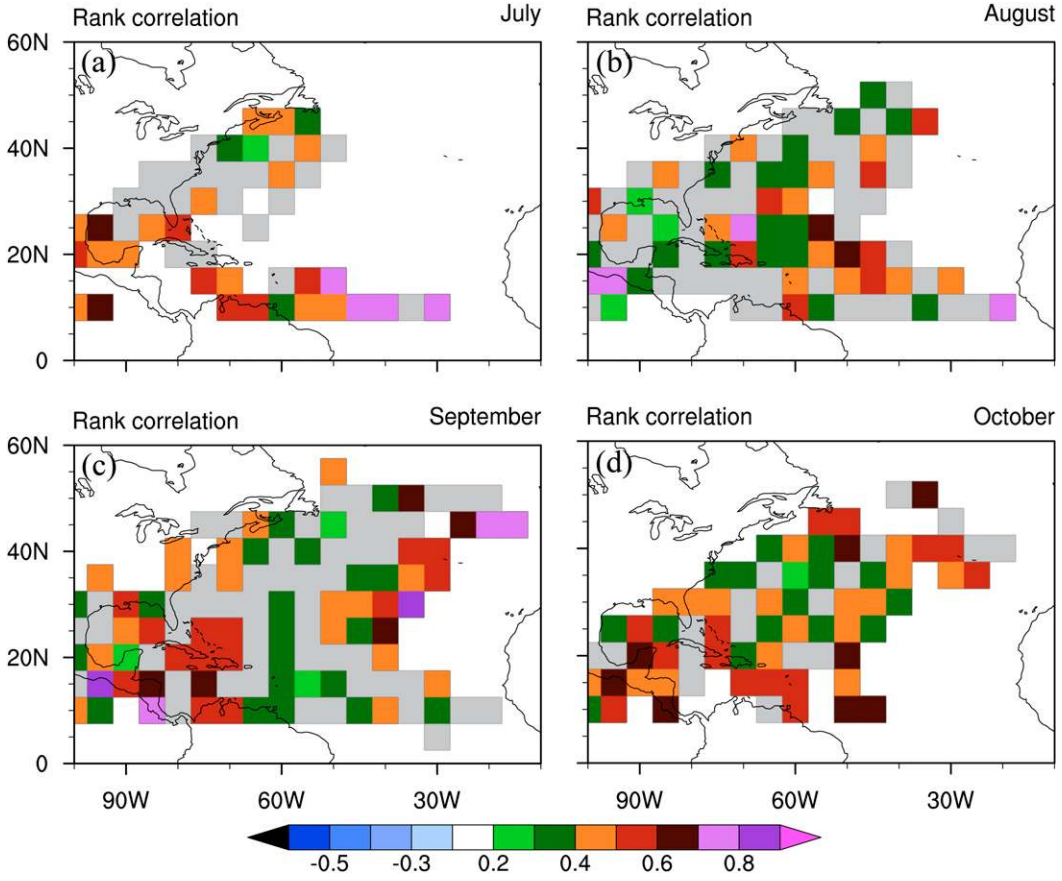

FIG. A3. As in Fig. 14, but for the NA.

between IBTrACS and the hindcast of FGOALS-f2 V1.0 is shown in Fig. A3.

REFERENCES

Alessandri, A., A. Borrelli, S. Gualdi, E. Scoccimarro, and S. Masina, 2011: Tropical cyclone count forecasting using a dynamical seasonal prediction system: Sensitivity to improved ocean initialization. *J. Climate*, **24**, 2963–2982, https://doi.org/10.1175/2010JCLI3585.1.

Arribas, A., and Coauthors, 2011: The GloSea4 ensemble prediction system for seasonal forecasting. *Mon. Wea. Rev.*, **139**, 1891–1910, https://doi.org/10.1175/2010MWR3615.1.

Baldwin, J. W., G. A. Vecchi, and S.Bordoni, 2019: The direct and ocean-mediated influence of Asian orography on tropical precipitation and cyclones. *Climate Dyn.*, **53**, 805–824, https://doi.org/10.1007/s00382-019-04615-5.

Banzon, V., T. M. Smith, T. M. Chin, C. Liu, and W. Hankins, 2016: A long-term record of blended satellite and in situ sea-surface temperature for climate monitoring, modeling and environmental studies. *Earth Syst. Sci. Data*, **8**, 165–176, https://doi.org/10.5194/essd-8-165-2016.

Bao, Q., and J. Li, 2020: Progress in climate modeling of precipitation over the Tibetan Plateau. *Natl. Sci. Rev.*, **7**, 486–487, https://doi.org/10.1093/nsr/nwaa006.

——, X. Wu, J. Li, L. Wang, B. He, X. Wang, Y. Liu, and G. Wu, 2018: Outlook for El Niño and the Indian Ocean dipole in autumn-winter 2018–2019. *Chin. Sci. Bull.*, **64**, 73–78, https://doi.org/10.1360/N972018-00913.

——, and Coauthors, 2020: CAS FGOALS-f3-H and CAS FGOALS-f3-L outputs for the high-resolution model intercomparison project simulation of CMIP6. *Atmos. Ocean. Sci. Lett.*, **13**, 576–581, https://doi.org/10.1080/16742834.2020.1814675.

Bloom, S., L. Takacs, A. Da Silva, and D. Ledvina, 1996: Data assimilation using incremental analysis updates. *Mon. Wea. Rev.*, **124**, 1256–1271, https://doi.org/10.1175/1520-0493(1996)124<1256:DAUIAU>2.0.CO;2.

Camargo, S. J., and A. H. Sobel, 2005: Western North Pacific tropical cyclone intensity and ENSO. *J. Climate*, **18**, 2996–3006, https://doi.org/10.1175/JCLI3457.1.

——, and A. A. Wing, 2016: Tropical cyclones in climate models. *Wiley Interdiscip. Rev.: Climate Change*, **7**, 211–237, https://doi.org/10.1002/wcc.373.

——, A. G. Barnston, P. J. Klotzbach, and C. W. Landsea, 2007a: Seasonal tropical cyclone forecasts. *WMO Bull.*, **56**, 297.

——, K. A. Emanuel, and A. H. Sobel, 2007b: Use of a genesis potential index to diagnose ENSO effects on tropical cyclone genesis. *J. Climate*, **20**, 4819–4834, https://doi.org/10.1175/JCLI4282.1.

——, and Coauthors, 2020: Characteristics of model tropical cyclone climatology and the large-scale environment. *J. Climate*, **33**, 4463–4487, https://doi.org/10.1175/JCLI-D-19-0500.1.

Camp, J., M. Roberts, C. MacLachlan, E. Wallace, L. Hermanson, A. Brookshaw, A. Arribas, and A. A. Scaife, 2015: Seasonal forecasting of tropical storms using the Met Office GloSea5 seasonal forecast system. *Quart. J. Roy. Meteor. Soc.*, **141**, 2206–2219, https://doi.org/10.1002/qj.2516.

——, and Coauthors, 2018: Skilful multiweek tropical cyclone prediction in ACCESS-S1 and the role of the MJO. *Quart. J. Roy. Meteor. Soc.*, **144**, 1337–1351, https://doi.org/10.1002/qj.3260.

——, and Coauthors, 2019: The western Pacific subtropical high and tropical cyclone landfall: Seasonal forecasts using the Met Office GloSea5 system. *Quart. J. Roy. Meteor. Soc.*, **145**, 105–116, https://doi.org/10.1002/qj.3407.

Chakraborty, P., A. Sarkar, S. Kumar, J. P. George, E. Rajagopal, and R. Bhatla, 2020: Assessment of NCMRWF global ensemble system with differing ensemble populations for tropical cyclone prediction. *Atmos. Res.*, **244**, 105077, https://doi.org/10.1016/j.atmosres.2020.105077.

Chan, J. C., J.-E. Shi, and C. Lam, 1998: Seasonal forecasting of tropical cyclone activity over the western North Pacific and the South China Sea. *Wea. Forecasting*, **13**, 997–1004, https://doi.org/10.1175/1520-0434(1998)013<0997:SFOTCA>2.0.CO;2.

Chen, G., 2011: How does shifting Pacific Ocean warming modulate on tropical cyclone frequency over the South China Sea? *J. Climate*, **24**, 4695–4700, https://doi.org/10.1175/2011JCLI4140.1.

Chen, J.-H., and S.-J. Lin, 2013: Seasonal predictions of tropical cyclones using a 25-km-resolution general circulation model. *J. Climate*, **26**, 380–398, https://doi.org/10.1175/JCLI-D-12-00061.1.

——, ——, L. Zhou, X. Chen, S. Rees, M. Bender, and M. Morin, 2019a: Evaluation of tropical cyclone forecasts in the next generation global prediction system. *Mon. Wea. Rev.*, **147**, 3409–3428, https://doi.org/10.1175/MWR-D-18-0227.1.

——, and Coauthors, 2019b: Advancements in hurricane prediction with NOAA's next-generation forecast system. *Geophys. Res. Lett.*, **46**, 4495–4501, https://doi.org/10.1029/2019GL082410.

Choi, K.-S., C.-C. Wu, and Y. Wang, 2014: Seasonal prediction for tropical cyclone frequency around Taiwan using teleconnection patterns. *Theor. Appl. Climatol.*, **116**, 501–514, https://doi.org/10.1007/s00704-013-0954-5.

Choi, W., C.-H. Ho, C.-S. Jin, J. Kim, S. Feng, D.-S. R. Park, and J.-K. E. Schemm, 2016: Seasonal forecasting of intense tropical cyclones over the North Atlantic and the western North Pacific basins. *Climate Dyn.*, **47**, 3063–3075, https://doi.org/10.1007/s00382-016-3013-y.

Chu, J.-H., C. R. Sampson, A. S. Levine, and E. Fukada, 2002: The joint typhoon warning center tropical cyclone best-tracks, 1945–2000. Ref. NRL/MR/7540-02, 16 pp.

Davis, K., and X. Zeng, 2019: Seasonal prediction of North Atlantic accumulated cyclone energy and major hurricane activity. *Wea. Forecasting*, **34**, 221–232, https://doi.org/10.1175/WAF-D-18-0125.1.

Dee, D. P., and Coauthors, 2011: The ERA-Interim reanalysis: Configuration and performance of the data assimilation system. *Quart. J. Roy. Meteor. Soc.*, **137**, 553–597, https://doi.org/10.1002/qj.828.

Domeisen, D. I., A. H. Butler, K. Fröhlich, M. Bittner, W. A. Müller, and J. Baehr, 2015: Seasonal predictability over Europe arising from El Niño and stratospheric variability in the MPI-ESM seasonal prediction system. *J. Climate*, **28**, 256–271, https://doi.org/10.1175/JCLI-D-14-00207.1.

Emanuel, K., 1995: Sensitivity of tropical cyclones to surface exchange coefficients and a revised steady-state model incorporating eye dynamics. *J. Atmos. Sci.*, **52**, 3969–3976, https://doi.org/10.1175/1520-0469(1995)052<3969:SOTCTS>2.0.CO;2.

——, and D. S. Nolan, 2004: Tropical cyclone activity and the global climate system. 26th Conf. on Hurricanes and Tropical Meteorolgy, Miami, FL, Amer. Meteor. Soc., 10A.2, https://ams.confex.com/ams/26HURR/techprogram/paper_75463.htm.

——, and A. Sobel, 2013: Response of tropical sea surface temperature, precipitation, and tropical cyclone-related variables to changes in global and local forcing. *J. Adv. Model. Earth Syst.*, **5**, 447–458, https://doi.org/10.1002/jame.20032.

Eyring, V., S. Bony, G. A. Meehl, C. A. Senior, B. Stevens, R. J. Stouffer, and K. E. Taylor, 2016: Overview of the Coupled

Model Intercomparison Project Phase 6 (CMIP6) experimental design and organization. *Geosci. Model Dev.*, **9**, 1937–1958, https://doi.org/10.5194/gmd-9-1937-2016.

Gao, K., J.-H. Chen, L. Harris, Y. Sun, and S.-J. Lin, 2019: Skillful prediction of monthly major hurricane activity in the North Atlantic with two-way nesting. *Geophys. Res. Lett.*, **46**, 9222–9230, https://doi.org/10.1029/2019GL083526.

Gray, W. M., 1984: Atlantic seasonal hurricane frequency. Part II: Forecasting its variability. *Mon. Wea. Rev.*, **112**, 1669–1683, https://doi.org/10.1175/1520-0493(1984)112<1669:ASHFPI>2.0.CO;2.

——, C. W. Landsea, P. W. Mielke Jr., and K. J. Berry, 1993: Predicting Atlantic basin seasonal tropical cyclone activity by 1 August. *Wea. Forecasting*, **8**, 73–86, https://doi.org/10.1175/1520-0434(1993)008<0073:PABSTC>2.0.CO;2.

——, ——, ——, and ——, 1994: Predicting Atlantic basin seasonal tropical cyclone activity by 1 June. *Wea. Forecasting*, **9**, 103–115, https://doi.org/10.1175/1520-0434(1994)009<0103:PABSTC>2.0.CO;2.

Haarsma, R. J., and Coauthors, 2016: High Resolution Model Intercomparison Project (HighResMIP v1. 0) for CMIP6. *Geosci. Model Dev.*, **9**, 4185–4208, https://doi.org/10.5194/gmd-9-4185-2016.

He, B., and Coauthors, 2019: CAS FGOALS-f3-L model datasets for CMIP6 historical atmospheric model intercomparison project simulation. *Adv. Atmos. Sci.*, **36**, 771–778, https://doi.org/10.1007/s00376-019-9027-8.

Huang, B., Y. Xue, D. Zhang, A. Kumar, and M. J. McPhaden, 2010: The NCEP GODAS ocean analysis of the tropical Pacific mixed layer heat budget on seasonal to interannual time scales. *J. Climate*, **23**, 4901–4925, https://doi.org/10.1175/2010JCLI3373.1.

Hunke, E., W. Lipscomb, A. Turner, N. Jeffery, and S. Elliott, 2008: CICE: The Los Alamos sea ice model, documentation and software, version 4.0. Los Alamos National Laboratory Tech. Rep. LA-CC-06-012, https://www.cesm.ucar.edu/models/ccsm4.0/cice/.

Jia, L., and Coauthors, 2015: Improved seasonal prediction of temperature and precipitation over land in a high-resolution GFDL climate model. *J. Climate*, **28**, 2044–2062, https://doi.org/10.1175/JCLI-D-14-00112.1.

Kerbyson, D. J., and P. W. Jones, 2005: A performance model of the parallel ocean program. *Int. J. High Perform. Comput. Appl.*, **19**, 261–276, https://doi.org/10.1177/1094342005056114.

Kim, H.-M., P. J. Webster, and J. A. Curry, 2009: Impact of shifting patterns of Pacific Ocean warming on North Atlantic tropical cyclones. *Science*, **325**, 77–80, https://doi.org/10.1126/science.1174062.

Klotzbach, P., and Coauthors, 2019: Seasonal tropical cyclone forecasting. *Trop. Cyclone Res. Rev.*, **8**, 134–149, https://doi.org/10.1016/j.tcrr.2019.10.003.

Knapp, K. R., M. C. Kruk, D. H. Levinson, H. J. Diamond, and C. J. Neumann, 2010: The International Best Track Archive for Climate Stewardship (IBTrACS) unifying tropical cyclone data. *Bull. Amer. Meteor. Soc.*, **91**, 363–376, https://doi.org/10.1175/2009BAMS2755.1.

Knutson, T. R., and Coauthors, 2010: Tropical cyclones and climate change. *Nat. Geosci.*, **3**, 157–163, https://doi.org/10.1038/ngeo779.

Kobayashi, S., and Coauthors, 2015: The JRA-55 reanalysis: General specifications and basic characteristics. *J. Meteor. Soc. Japan*, **93**, 5–48, https://doi.org/10.2151/jmsj.2015-001.

Landsea, C. W., and J. L. Franklin, 2013: Atlantic hurricane database uncertainty and presentation of a new database format. *Mon. Wea. Rev.*, **141**, 3576–3592, https://doi.org/10.1175/MWR-D-12-00254.1.

Lawrence, D. M., and Coauthors, 2011: Parameterization improvements and functional and structural advances in version 4 of the community land model. *J. Adv. Model. Earth Syst.*, **3**, M03001, https://doi.org/10.1029/2011MS00045.

Li, J., Q. Bao, Y. Liu, and G. Wu, 2017: Evaluation of the computational performance of the finite-volume atmospheric model of the IAP/LASG (FAMIL) on a high-performance computer. *Atmos. Ocean. Sci. Lett.*, **10**, 329–336, https://doi.org/10.1080/16742834.2017.1331111.

——, ——, ——, ——, L. Wang, B. He, X. Wang, and J. Li, 2019: Evaluation of FAMIL2 in simulating the climatology and seasonal-to-interannual variability of tropical cyclone characteristics. *J. Adv. Model. Earth Syst.*, **11**, 1117–1136, https://doi.org/10.1029/2018MS001506.

Li, W., Z. Wang, and M. S. Peng, 2016: Evaluating tropical cyclone forecasts from the NCEP Global Ensemble Forecasting System (GEFS) reforecast version 2. *Wea. Forecasting*, **31**, 895–916, https://doi.org/10.1175/WAF-D-15-0176.1.

Lin, S.-J., 2004: A "vertically Lagrangian" finite-volume dynamical core for global models. *Mon. Wea. Rev.*, **132**, 2293–2307, https://doi.org/10.1175/1520-0493(2004)132<2293:AVLFDC>2.0.CO;2.

MacLachlan, C., and Coauthors, 2015: Global Seasonal Forecast System version 5 (GloSea5): A high-resolution seasonal forecast system. *Quart. J. Roy. Meteor. Soc.*, **141**, 1072–1084, https://doi.org/10.1002/qj.2396.

Manganello, J. V., and Coauthors, 2012: Tropical cyclone climatology in a 10-km global atmospheric GCM: Toward weather-resolving climate modeling. *J. Climate*, **25**, 3867–3893, https://doi.org/10.1175/JCLI-D-11-00346.1.

——, and Coauthors, 2014: Future changes in the western North pacific tropical cyclone activity projected by a multidecadal simulation with a 16-km global atmospheric GCM. *J. Climate*, **27**, 7622–7646, https://doi.org/10.1175/JCLI-D-13-00678.1.

——, and Coauthors, 2016: Seasonal forecasts of tropical cyclone activity in a high-atmospheric-resolution coupled prediction system. *J. Climate*, **29**, 1179–1200, https://doi.org/10.1175/JCLI-D-15-0531.1.

——, B. A. Cash, K. I. Hodges, and J. L. Kinter, 2019: Seasonal forecasts of North Atlantic tropical cyclone activity in the North American multi-model ensemble. *Climate Dyn.*, **53**, 7169–7184, https://doi.org/10.1007/s00382-017-3670-5.

Mason, S. J., L. Goddard, N. E. Graham, E. Yulaeva, L. Sun, and P. A. Arkin, 1999: The IRI seasonal climate prediction system and the 1997/98 El Niño event. *Bull. Amer. Meteor. Soc.*, **80**, 1853–1873, https://doi.org/10.1175/1520-0477(1999)080<1853:TISCPS>2.0.CO;2.

Moon, I.-J., S.-H. Kim, and C. Wang, 2015: El Niño and intense tropical cyclones. *Nature*, **526**, E4–E5, https://doi.org/10.1038/nature15546.

Murakami, H., and M. Sugi, 2010: Effect of model resolution on tropical cyclone climate projections. *SOLA*, **6**, 73–76, https://doi.org/10.2151/sola.2010-019.

——, and Coauthors, 2012: Future changes in tropical cyclone activity projected by the new high-resolution MRI-AGCM. *J. Climate*, **25**, 3237–3260, https://doi.org/10.1175/JCLI-D-11-00415.1.

——, and Coauthors, 2015: Simulation and prediction of category 4 and 5 hurricanes in the high-resolution GFDL HIFLOR coupled climate model. *J. Climate*, **28**, 9058–9079, https://doi.org/10.1175/JCLI-D-15-0216.1.

——, G. Villarini, G. A. Vecchi, W. Zhang, and R. Gudgel, 2016a: Statistical–dynamical seasonal forecast of North Atlantic and us landfalling tropical cyclones using the high-resolution GFDL FLOR coupled model. *Mon. Wea. Rev.*, **144**, 2101–2123, https://doi.org/10.1175/MWR-D-15-0308.1.

——, and Coauthors, 2016b: Seasonal forecasts of major hurricanes and landfalling tropical cyclones using a high-resolution GFDL coupled climate model. *J. Climate*, **29**, 7977–7989, https://doi.org/10.1175/JCLI-D-16-0233.1.

——, E. Levin, T. Delworth, R. Gudgel, and P.-C. Hsu, 2018: Dominant effect of relative tropical Atlantic warming on major hurricane occurrence. *Science*, **362**, 794–799, https://doi.org/10.1126/science.aat6711.

Nath, S., and Coauthors, 2015: Seasonal prediction of tropical cyclone activity over the north Indian Ocean using the neural network model. *Atmósfera*, **28**, 271–281, https://doi.org/10.20937/ATM.2015.28.04.06.

Nicholls, N., 1979: A possible method for predicting seasonal tropical cyclone activity in the Australian region. *Mon. Wea. Rev.*, **107**, 1221–1224, https://doi.org/10.1175/1520-0493(1979)107<1221:APMFPS>2.0.CO;2.

Oleson, K. W., and Coauthors, 2010: Technical description of version 4.0 of the Community Land Model (CLM). NCAR Tech. Note NCAR/TN-478+STR, 257 pp., https://doi.org/10.5065/D6FB50WZ.

Oouchi, K., J. Yoshimura, H. Yoshimura, R. Mizuta, S. Kusunoki, and A. Noda, 2006: Tropical cyclone climatology in a global-warming climate as simulated in a 20 km-mesh global atmospheric model: Frequency and wind intensity analyses. *J. Meteor. Soc. Japan*, **84**, 259–276, https://doi.org/10.2151/jmsj.84.259.

Putman, W. M., and S.-J. Lin, 2007: Finite-volume transport on various cubed-sphere grids. *J. Comput. Phys.*, **227**, 55–78, https://doi.org/10.1016/j.jcp.2007.07.022.

Ren, H.-L., and Coauthors, 2019: The China multi-model ensemble prediction system and its application to flood-season prediction in 2018. *J. Meteor. Res.*, **33**, 540–552, https://doi.org/10.1007/s13351-019-8154-6.

Reynolds, R. W., T. M. Smith, C. Liu, D. B. Chelton, K. S. Casey, and M. G. Schlax, 2007: Daily high-resolution-blended analyses for sea surface temperature. *J. Climate*, **20**, 5473–5496, https://doi.org/10.1175/2007JCLI1824.1.

Shaevitz, D. A., and Coauthors, 2014: Characteristics of tropical cyclones in high-resolution models in the present climate. *J. Adv. Model. Earth Syst.*, **6**, 1154–1172, https://doi.org/10.1002/2014MS000372.

Simpson, R. H., and H. Saffir, 1974: The hurricane disaster—potential scale. *Weatherwise*, **27**, 169–186, https://doi.org/10.1080/00431672.1974.9931702.

Small, R. J., and Coauthors, 2014: A new synoptic scale resolving global climate simulation using the community earth system model. *J. Adv. Model. Earth Syst.*, **6**, 1065–1094, https://doi.org/10.1002/2014MS000363.

Strachan, J., P. L. Vidale, K. Hodges, M. Roberts, and M.-E. Demory, 2013: Investigating global tropical cyclone activity with a hierarchy of AGCMS: The role of model resolution. *J. Climate*, **26**, 133–152, https://doi.org/10.1175/JCLI-D-12-00012.1.

Tang, B. H., and J. Neelin, 2004: Enso influence on Atlantic hurricanes via tropospheric warming. *Geophys. Res. Lett.*, **31**, L24204, https://doi.org/10.1029/2004GL021072.

Vecchi, G. A., and Coauthors, 2014: On the seasonal forecasting of regional tropical cyclone activity. *J. Climate*, **27**, 7994–8016, https://doi.org/10.1175/JCLI-D-14-00158.1.

Villarini, G., B. Luitel, G. A. Vecchi, and J. Ghosh, 2019: Multimodel ensemble forecasting of North Atlantic tropical cyclone activity. *Climate Dyn.*, **53**, 7461–7477, https://doi.org/10.1007/s00382-016-3369-z.

Vitart, F., 2014: Evolution of ECMWF sub-seasonal forecast skill scores. *Quart. J. Roy. Meteor. Soc.*, **140**, 1889–1899, https://doi.org/10.1002/qj.2256.

——, and A. W. Robertson, 2018: The sub-seasonal to seasonal prediction project (s2s) and the prediction of extreme events. *NPJ Climate Atmos. Sci.*, **1**, 3, https://doi.org/10.1038/s41612-018-0013-0.

——, D. Anderson, and T. Stockdale, 2003: Seasonal forecasting of tropical cyclone landfall over Mozambique. *J. Climate*, **16**, 3932–3945, https://doi.org/10.1175/1520-0442(2003)016<3932:SFOTCL>2.0.CO;2.

——, and Coauthors, 2017: The Subseasonal to Seasonal (S2S) prediction project database. *Bull. Amer. Meteor. Soc.*, **98**, 163–173, https://doi.org/10.1175/BAMS-D-16-0017.1.

Walsh, K. J., and Coauthors, 2016: Tropical cyclones and climate change. *Wiley Interdiscip. Rev.: Climate Change*, **7**, 65–89, https://doi.org/10.1002/wcc.371.

Wang, B., and J. C. Chan, 2002: How strong ENSO events affect tropical storm activity over the western North Pacific. *J. Climate*, **15**, 1643–1658, https://doi.org/10.1175/1520-0442(2002)015<1643:HSEEAT>2.0.CO;2.

——, B. Xiang, and J.-Y. Lee, 2013: Subtropical high predictability establishes a promising way for monsoon and tropical storm predictions. *Proc. Natl. Acad. Sci. USA*, **110**, 2718–2722, https://doi.org/10.1073/pnas.1214626110.

Wang, H., and Coauthors, 2015: A review of seasonal climate prediction research in China. *Adv. Atmos. Sci.*, **32**, 149–168, https://doi.org/10.1007/s00376-014-0016-7.

Wang, L., Q. Bao, J. Li, D. Wang, Y. Liu, G. Wu, and X. Wu, 2019a: Comparisons of the temperature and humidity profiles of reanalysis products with shipboard GPS sounding measurements obtained during the 2018 Eastern Indian Ocean open cruise. *Atmos. Oceanic Sci. Lett.*, **12**, 177–183, https://doi.org/10.1080/16742834.2019.1588065.

——, and Coauthors, 2019b: LASG global AGCM with a two-moment cloud microphysics scheme: Energy balance and cloud radiative forcing characteristics. *Adv. Atmos. Sci.*, **36**, 697–710, https://doi.org/10.1007/s00376-019-8196-9.

Wu, G., and N.-C. Lau, 1992: A GCM simulation of the relationship between tropical-storm formation and ENSO. *Mon. Wea. Rev.*, **120**, 958–977, https://doi.org/10.1175/1520-0493(1992)120<0958:AGSOTR>2.0.CO;2.

Xiang, B., and Coauthors, 2015: Beyond weather time-scale prediction for Hurricane Sandy and Super Typhoon Haiyan in a global climate model. *Mon. Wea. Rev.*, **143**, 524–535, https://doi.org/10.1175/MWR-D-14-00227.1.

Ying, M., W. Zhang, H. Yu, X. Lu, J. Feng, Y. Fan, Y. Zhu, and D. Chen, 2014: An overview of the China Meteorological Administration tropical cyclone database. *J. Atmos. Oceanic Technol.*, **31**, 287–301, https://doi.org/10.1175/JTECH-D-12-00119.1.

Zhang, W., and G. Villarini, 2019: Seasonal forecasting of western North Pacific tropical cyclone frequency using the North American multi-model ensemble. *Climate Dyn.*, **52**, 5985–5997, https://doi.org/10.1007/s00382-018-4490-y.

——, and Coauthors, 2016: Improved simulation of tropical cyclone responses to ENSO in the western North Pacific in the high-resolution GFDL HIFLOR coupled climate model. *J. Climate*, **29**, 1391–1415, https://doi.org/10.1175/JCLI-D-15-0475.1.

——, G. A. Vecchi, G. Villarini, H. Murakami1, R. Gudgel, and X. Yang, 2017: Statistical–dynamical seasonal forecast of western North Pacific and East Asia landfalling tropical cyclones using the GFDL FLOR coupled climate model. *J. Climate*, **30**, 2209–2232, https://doi.org/10.1175/JCLI-D-16-0487.1.

Zhao, C., H.-L. Ren, R. Eade, Y. Wu, J. Wu, and C. MacLachlan, 2019: MJO modulation and its ability to predict boreal summer tropical cyclone genesis over the northwest Pacific in Met Office Hadley Centre and Beijing climate center seasonal prediction systems. *Quart. J. Roy. Meteor. Soc.*, **145**, 1089–1101, https://doi.org/10.1002/qj.3478.

Zhao, M., I. M. Held, and S.-J. Lin, 2009: Simulations of global hurricane climatology, interannual variability, and response to global warming using a 50-km resolution GCM. *J. Climate*, **22**, 6653–6678, https://doi.org/10.1175/2009JCLI3049.1.

——, and Coauthors, 2018a: The GFDL global atmosphere and land model AM4.0/LM4.0: 1. Simulation characteristics with prescribed SSTs. *J. Adv. Model. Earth Syst.*, **10**, 691–734, https://doi.org/10.1002/2017MS001208.

——, and Coauthors, 2018b: The GFDL global atmosphere and land model AM4.0/LM4.0: 2. Model description, sensitivity studies, and tuning strategies. *J. Adv. Model. Earth Syst.*, **10**, 735–769, https://doi.org/10.1002/2017MS001209.

Zhou, L., Y. Liu, Q. Bao, H. Yu, and G. Wu, 2012: Computational performance of the high-resolution atmospheric model FAMIL. *Atmos. Oceanic Sci. Lett.*, **5**, 355–359, https://doi.org/10.1080/16742834.2012.11447024.

——, and Coauthors, 2015: Global energy and water balance: Characteristics from finite-volume atmospheric model of the IAP/LASG (FAMIL 1). *J. Adv. Model. Earth Syst.*, **7**, 1–20, https://doi.org/10.1002/2014MS000349.

——, S.-J. Lin, J.-H. Chen, L. M. Harris, X. Chen, and S. L. Rees, 2019: Toward convective-scale prediction within the next generation global prediction system. *Bull. Amer. Meteor. Soc.*, **100**, 1225–1243, https://doi.org/10.1175/BAMS-D-17-0246.1.

Zhou, T., and Coauthors, 2016: GMMIP (v1. 0) contribution to CMIP6: Global monsoons model inter-comparison project. *Geosci. Model Dev.*, **9**, 3589–3604, https://doi.org/10.5194/gmd-9-3589-2016.